MAJOR SPACE WEATHER EVENT REPORT FROM ESA SPACE WEATHER NETWORK

Prepared by	The ESA SWE Network
Document Type	Report
Reference	S2P-SWE-S1SW256-PROJ-RP-0003
Issue/Revision	1.2
Date of Issue	06/02/2025
Status	Approved

APPROVAL

Title	MAJOR SPACE WEATHER EVENT REPORT FROM ESA SPACE WEATHER NETWORK		
Issue Number	1	Revision Number	2
Author	The ESA SWE Network	Date	06/02/2025
Approved By		Date of Approval	
	SSCC Coordinator	Jennifer O'Hara Digitally signed by Jennifer O'Hara Date: 2025.05.28 16:03:27 +02'00'	
	SWESNET Project Manager	Alice Michel Digitally signed by Alice Michel DN: cn=Alice Michel, o, ou, email=alice.michel@aeronomie.be, c=BE Date: 2025.06.02 13:18:46 +02'00'	
	ESA Technical Officer	Alexi Glover Digitally signed by Alexi Glover Date: 2025.06.18 17:42:36 +02'00'	

CHANGE LOG

Reason for change	Issue Nr	Revision Number	Date
Initial issue	1	0	21/06/2024
Update after ESA review	1	1	16/12/2024
Update after ESA review	1	2	06/02/2025

CHANGE RECORD

Issue Number 1	Revision Number 2		
Reason for change	Date	Pages	Paragraph(s)
Adressing the feedback from ESA	06/02/2025	All	

DISTRIBUTION

Name/Organisational Unit

Table of Contents

1 INTRODUCTION

1.1 Purpose of the document

This document has been prepared in the frame of the Space Weather Service Network Development and Pre-Operation Part 1 (S2P-S1-SW-02.2, S1-SW-05, S1-SW-06) project later referred to as SWESNET.

This document provides a report on a major space weather event from the ESA Space Weather Service Network, and it has been constructed by the ESA Space Weather Coordination Centre (SSCC) based on input from the ESCs.
This document has been prepared by the ESA SWE Network in the frame of ESA Contract No. 4000134036/21/D/MRP with contribution from: Camilla Scolini (ROB), Chris Perry (STFC), Norma B. Crosby (BIRA-IASB), Martin Kriegel (DLR), Paul David (DLR), Line Drube (DTU), Anna Willer (DTU) Judith de Patoul (ROB), Jennifer O'Hara (ROB), Robbe Vansintjan (ROB) with input from Expert Groups (EGs) part of the S-ESC, H-ESC, R-ESC, I-ESC, and G-ESC.

1.2 References

1.2.1 Applicable documents

ID	Document Title	Reference, Issue, Date
[AD-SOW]	Space Weather Service Network Development And Pre-Operation Part 1 (S2P - S1-SW-02.2, S1-SW-05, S1-SW-06) – Statement of Work	ESA-S2P-SWE-SOW-0003, i1r0, July 1, 2020

1.2.2 Reference documents

ID	Document Title	Reference, Issue, Date
[RD-PROD]	ESA Space Weather Coordination Centre Product Catalogue Summary	SSA-SWE-SSCC-TN-0011 Issue 21 rev 0, 13/06/2024
[RD-COM]	ESA SWE Consistent Communications Protocol	S2P-SWE-S1SW256-SSCC-TN-0001 Issue 6 rev 4, 06/03/2023

1.2.3 Acronyms and Abbreviations

AD	Applicable Document
AIA	Atmospheric Imaging Assembly
AR	Active Region
API	Application Programming Interface
AWT	Advanced Warning Time
CME	Coronal Mass Ejection
DBEM	Drag-Based Ensemble Model
ECSS	European Co-operation for Space Standardisation
EG	Export Group
ESC	Expert Service Centre
ESD	Electrostatic Discharge
GEO	Geosynchronous Equatorial Orbit
GIC	Geomagnetic Induced Currents
IMF	Interplanetary Magnetic Field
LCDS	Last Closed Drift Shell
LDE	Long Duration Event
LEO	Low Earth Orbit
LSTIDs	Large Scale Traveling Ionospheric Disturbances
MLT	Magnetic Local Time
MUF	Maximum Usable Frequency
N/A	Not Applicable
PCN	Polar Cap North
PDF	Portable Document Format
RD	Reference Document
SDO	Solar Dynamics Observatory
SPE	Solar Particle Event
SOW	Statement of Work
SSA	Space Situational Awareness
SSCC	SSA Space Weather Coordination Centre
TEC	Total Electron Content
ROTI	Rate of TEC Index
UTC	Coordinated Universal Time
VTEC	Vertical TEC

2 BACKGROUND INFORMATION / APPROACH

This report contains a Space Weather Event Summary from the ESA Space Weather Network (hereafter, “the network”), and was constructed by the SSA Space Weather Coordination Centre (SSCC) based on input form the Expert Service Centres (ESCs) part of the network. This report was compiled by the SSCC as a consolidated post-event analysis based on input from the ESCs and EGs belonging to the network.

The report covers a major space weather event that took place between 21 April 2023 and 25 April 2023 and the associated impacts thereafter. The choice of this event was based on a number of considerations: the event was associated with one of the strongest geomagnetic storms of current solar cycle 25 (reaching a maximum Kp value of 8+); the event provided an excellent example to showcase a variety of impacts affecting multiple products in the network. Furthermore, the event received considerable press and media coverage. The report also demonstrates the capabilities of the network in capturing major space weather events, showing how the full detail of the such a major space weather event can be seen and tracked via the ESA SWE Portal from the first solar eruption and early impact predictions, up to the actual impact at Earth.

2.1 Conclusions and Lessions Learnt

This report was created to provide a consolidated description of the event, highlighting the breadth of the data available on the portal as well as attempting to summarize how the impact could be seen by users in the relevant data. As a post-event analysis, this report is able to explore the timeline of the event in detail and make connections between the different data sources as well as enabling retrospective analysis on how this event was predicted by the network forecasts and models. It should be noted that this is therefore a very different exercise and output compared to the messages created as part of the network communication exercises [RD-COM], which are designed to be made in real time for extreme space weather events which surpass specified thresholds. Although the two processes are distinct from each other and have separate timelines for their compilation and different objectives, which should not be confused, we can also see that the compilation of such event summary reports as this made post factum can also help provide interesting examples and training for the network in the future description of such events, and could help inform the language used or standard texts prepared in the framework of the communication exercises.

This report is a detailed description of the event from April 2023 and draws from products in the entire network to provide a full overview. However, this also means that this report covers multiple areas of interest and describes multiple impacts. In the future, a more precise pre-scription of an event report would help to make a more focused output. For example, if such reports are proposed for future developments, it could be beneficial to limit the scope to focus on how an event is covered for one service or service domain.

Additionally, an agreement on how to choose such an event would enable such reports to be produced sooner after events have taken place (although not in real time), which would also allow the Network to show that they are able to provide up to date interesting content, that if needed could be adapted for presentation to users where effort is foreseen.

3 EVENT DESCRIPTION AND IMPACTS

3.1 Short Summary

A violent eruption took place on the Sun on 21 April 2023 from active region NOAA AR 13283. The eruption was associated with a long duration M1.7 flare detected in soft X-rays by the GOES satellites, and in EUV. The eruption was the result of the interaction between a filament in NOAA AR 13283 and a much larger but quiescent filament to the east of this region. Post-eruption coronal loops and coronal dimming suggested the eruption of a coronal mass ejection (CME). A full halo CME was indeed observed by the SOHO/LASCO coronagraphs starting at 18:12 UTC. In their first bulletins, space weather forecasters at the SIDC and UK Met Office estimated a heads-on impact at Earth between late 23 April and early 24 April, possibly leading to Major Geomagnetic Storm G3 on the NOAA SWPC scale (later just reffered to Gn, n for number (Kp=7) conditions.

The CME arrival at Earth was observed at 16:59 UTC on 23 April, about 10 hours earlier than predicted by heliospheric propagation models, but within the uncertainty window (for example for the H.101z product). The interplanetary CME was characterized by a strong dynamic pressure and prolonged periods of negative Bz, triggering a stronger geomagnetic activity that initially forecasted (reaching a Severe Geomagnetic Storm G4 level -- Kp=8). Kp predictions for 23 April and 24 April made by Swedish Institute of Space Physics (IRF) with a few hours of lead time were consistent with Kp observations. However, on 24 April the Dst was significantly under-predicted compared to measured values, with forecasts reaching -100 nT compared to observations. An intense geomagnetic activity was recorded across northern Europe, including large amplitudes in the horizontal magnetic field intensity, large variations in the horizontal component of the magnetic field, and local-K values reaching values of 9.

Starting from around noon (UTC) on 23 April, the radiation environment at L1 and GEO was also affected by the approaching interplanetary CME. Electron events at L1 were observed at 16:58 UTC and 17:30 UTC on 23 April, while a proton event occurred at 17:44 UTC. A proton intensity alert level was issued by the HESPERIA REleASE at 17:30 UTC, with an warning time of only 15 minutes for this particular event.

The ionospheric environment and telecommunication systems relying on wave propagation through the ionosphere were also perturbed by this space weather event. A depletion in the Total Electron Content (TEC) was observed at high latitudes (>50° N) from 23 April at 18:00 UTC. A strong impact on GNSS across Norway was observed between 18:00 UTC on 23 April and 09:00 UTC on 24 April, as shown in the Rate of TEC Index (ROTI) at ground time series and maps. A strong depletion of the maximum usable frequency (MUF) was also observed from 23 April at 16:00 UTC to 24 April at 17:00 UTC. Several alerts were issued by various I-ESC products within the network between 23 April at 18:00 UTC and 24 April at 09:00 UTC. A strong probability of detection of large scale traveling ionospheric disturbances (LSTIDs), linked to the enhanced auroral activity, was indicated by TechTIDE TEC gradient maps.

Impacts on the electron and proton populations at lower altitudes (i.e. radiation belts and slot region) and on the risks for satellite electric charging extended over a longer time window, until 2 May i.e. throughout the week following the arrival of the interplanetary CME at Earth.

Finally, the network also captured in detail the impacts of this event on ground-based systems through products part of the G-ESC. Major Geomagnetic Induced Currents (GICs) were measured in northern Europe, reaching an estimated maximum value of 35 A - which ranks in the top 5 daily maximums since November 1998. Several periods indicate the estimated GICs exceeded the top 0.1% of all values in long-term statistics in 1996-2008.

3.2 Extended Report

A violent eruption took place on the Sun on 21 April 2023. The eruption took place in active region NOAA AR 13283 (Catania Region 61), which had a beta magnetic classification, as reported by the SIDC forecaster in product S.110 and exhibited only a few sunspots. **Figure 1** shows daily drawings of the sunspot group within NOAA AR 13283, and information about the evolution of the region in the days prior to the eruption as provided by product S.123a (INAF/OACT sunspot group characteristics, https://swe.ssa.esa.int/catania-S123a-federated). **Figure 2** shows images of the sun in H-alpha and demonstrates how in the days prior to the eruption, a complex filament system was visible in and around NOAA AR 13283 (from product S.122, INAF/OACT Halpha solar images, https://swe.ssa.esa.int/catania-S122-federated).

In the days prior to the eruption, active region NOAA AR 13283 was decaying. On 19 April, NOAA AR 3283 contained 4 spots and had a Cao McIntosh classification, indicating a bipolar sunspot group with at least one spot having a formed penumbra. While on 21 April, NOAA AR 13283 contained 10 small spots but had a Bxi classification, indicating a bipolar sunspot group with no penumbra. Such a decaying behaviour is confirmed also by product S.123d (ASUCAS/SPS sunspot group characteristics, https://swe.ssa.esa.int/sps-S123d-federated). Sunspot drawings are shown for the “latest” data only, but past drawings are available to download from product S.123a https://swe.ssa.esa.int/web/guest/catania-S123a-federated .

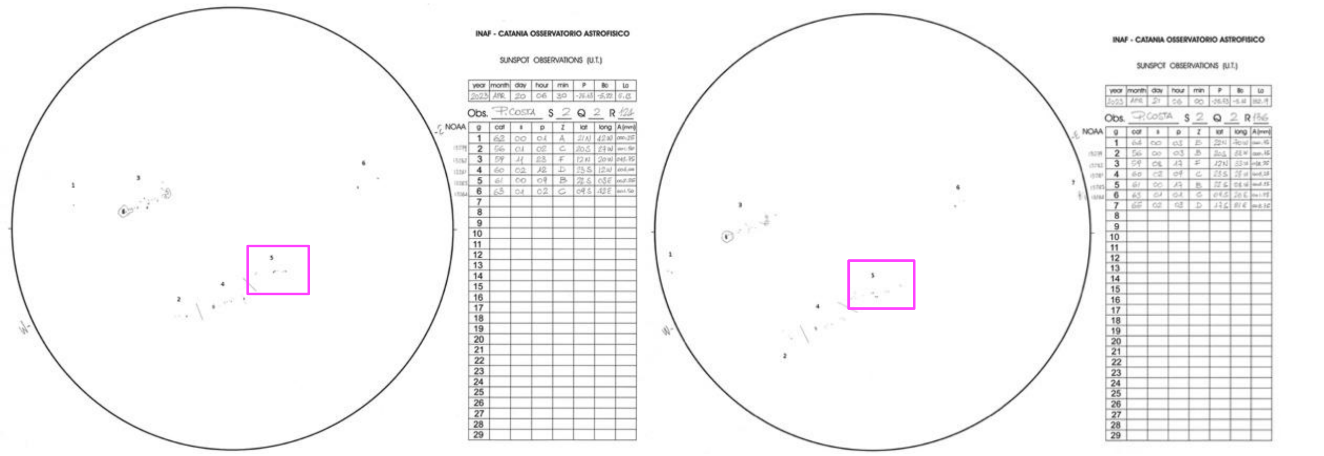

Figure 1: *INAF/OACT sunspot drawings for 20-21 April 2023, including a description of each sunspot's properties. NOAA AR 13283 is highlighted in magenta. From product S.123a.*

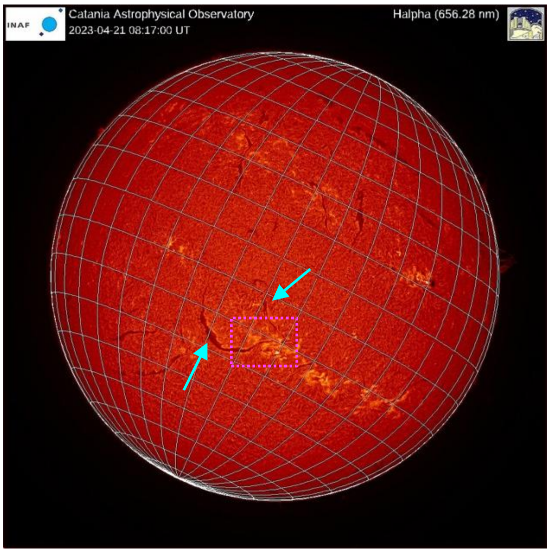

Figure 2: *INAF/OACT Halpha solar image on 21 April 2023 (prior to the eruption). NOAA AR 13283 is marked in magenta. The filament system related to NOAA AR 13283 is marked by the cyan arrows. From product S.122.*

Due to its low complexity and moderated flaring activity in the previous days, flare forecasts for NOAA AR 13283 on 21 April 2023 were conservative. For example, the on-duty ASUCAS forecaster predicted flaring at C/M/X level with 40%/5%/1% probability, as reported by product S.501a (ASUCAS/SPS solar flare forecast, https://swe.ssa.esa.int/sps-S501a-federated), compiled daily at 17:00 UTC and valid for the next 24 hours. Similarly, the on-duty SIDC forecaster predicted flaring at C+/M+/X level with 30%/5%/1% probability, as reported by product S.109b (SIDC flare forecast, https://swe.ssa.esa.int/sidc-S109b-federated), compiled daily at 12:00 UTC and valid for the next 24 hours. Despite a 5% flaring probability predicted for 21 April, an associated M1.7 flare was detected in soft X-rays by GOES satellites starting at 17:44 UTC (https://www.swpc.noaa.gov/products/goes-x-ray-flux). This classified as a long duration event (LDE), lasting about an hour and ending at 18:37 UTC. The peak time was at 18:12 UTC. An LDE flare was also detected by the SIDC Solar EUV Flare Detection (product S.127, https://swe.ssa.esa.int/sidc-S127-federated) automated flare detection tool in EUV wavelengths, where it was classified as an M1.1 flare (**Figure 3**). In EUV, the flare started at 17:54 UTC and ended at 18:42 UTC, with a peak time at 18:21 UTC.

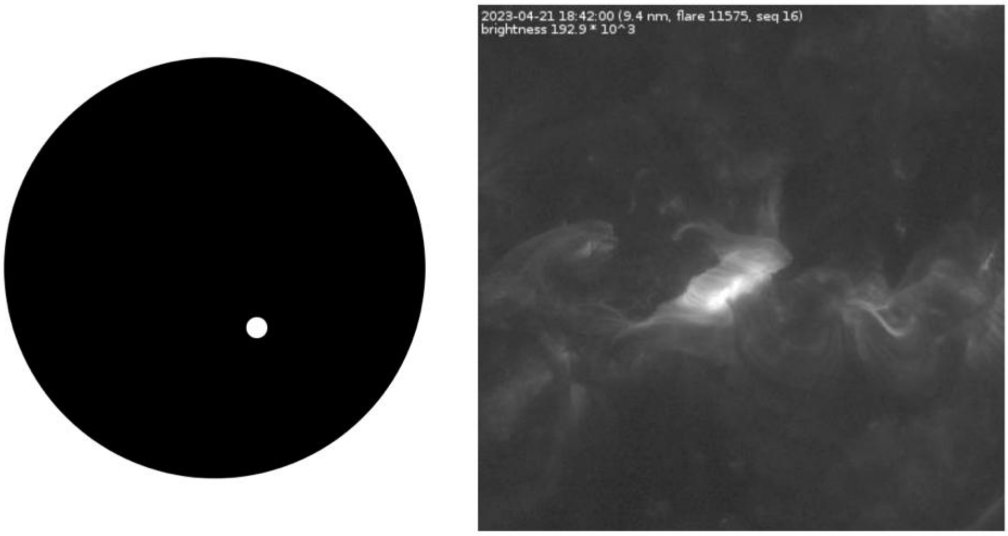

Figure 3: *EUV flare identification by the SIDC Solar EUV Flare Detection. Left: location of the flare on the solar disk. Right: EUV flare observation at 18:42 UTC (from SDO/AIA 94). From product S.127.*

Some electric current activity was visible in AR 13283, but the same was true also for AR 13279, and in both cases, currents were barely distinguishable from background noise. **Figure 4** shows current maps for the SDO/HMI "HARP" region 9374, which includes NOAA ARs 13276, 13279, 13281, and 13283 on 21 April, as provided by product S.052a (UPSaclay/MEDOC Maps of electric currents in active regions, https://swe.ssa.esa.int/medoc-S052a-federated).

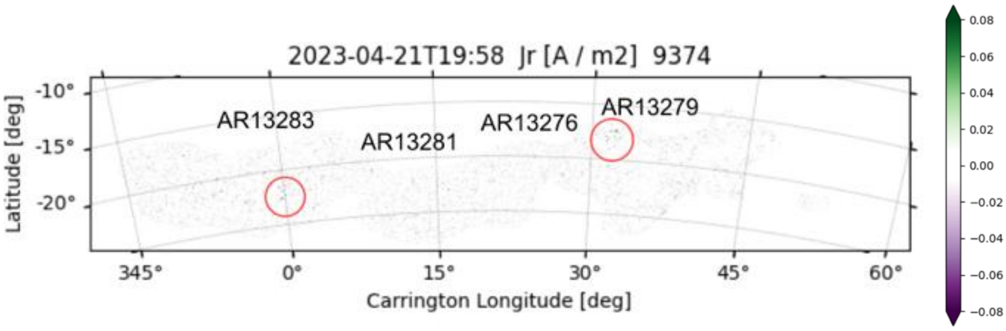

***Figure 4:** Current maps for the SDO/HMI "HARP" region 9374, including NOAA ARs 13276, 13279, 13281, and 13283 on 21 April at 19:58 UTC (after the flare). AR 13283 is located at the eastmost part of the maps. From product S.052a.*

The eruption was the result of the interaction between a filament in NOAA AR 13283 and a much larger but quiescent filament to the east of this region. Part of the group filament erupted, while part recomposed itself on the disk. SDO/AIA 304Å images, provided by product S.106 (SIDC SDO/AIA solar EUV images, https://swe.ssa.esa.int/sidc-S106-federated) show the filaments started being destabilized around 17:24 UTC, while the filament eruption occurred around 17:57 UTC (**Figure 5**).

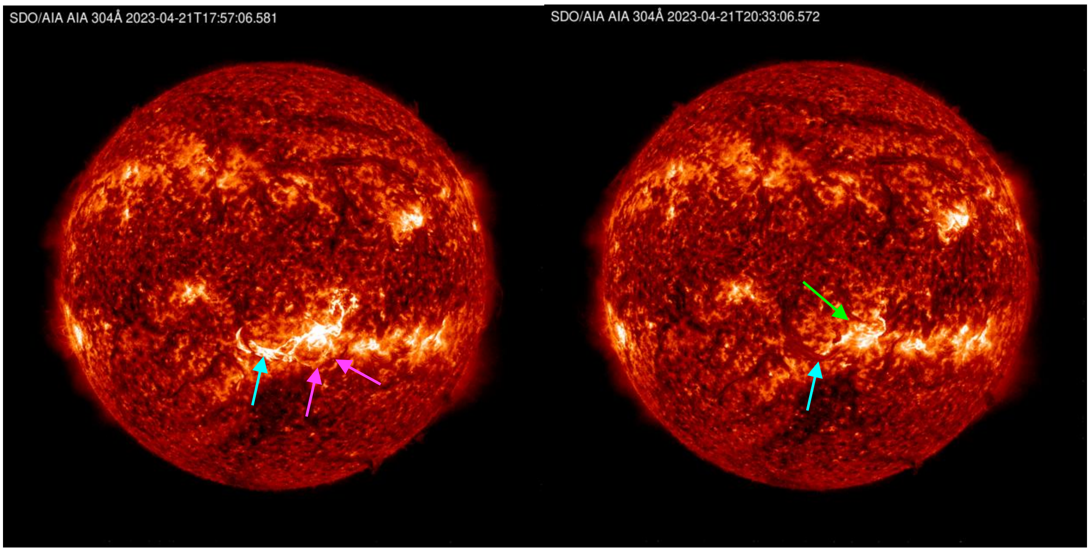

***Figure 5**: SDO/AIA 304Å images during the eruption. Left: image on 21 April 2023 at 17:57 UTC, with the large filament on the east highlighted by the cyan arrow, and the erupting part of the filament system of NOAA AR 3283 highlighted by magenta arrows. Right: image on 21 April 2023 at 20:33 UTC, after the large filament on the east has returned to its original position on the disk (in cyan). At this time, post-eruptive loops are visible above NOAA AR 3283 (marked by the green arrows). From product S.106.*

Figure 6 shows the mapped filaments on the solar disk, before and after eruption, as provided by Product S.107f (UNIGRAZ/KSO filament detection, https://swe.ssa.esa.int/kso-S107f-federated). On 21 April, one small filament overlying NOAA AR 13283, together with one large filament on the east of the active region, can be seen. On 22 April, the large filament to the east is still present, while the filament overlying NOAA AR 13283 has split into two smaller components, one in the north and one in the south part of the active region.

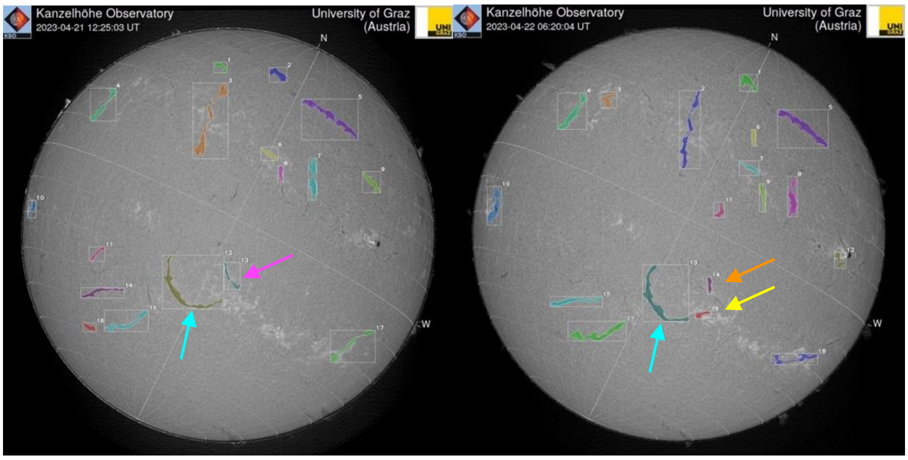

***Figure 6**: UNIGRAZ/KSO filament detection on 21 (left) and 22 (right) April 2023. The filament on the east of NOAA AR 3283 is marked in cyan, while the filament system within NOAA AR 3283 is marked in magenta prior to the eruption, and in yellow and orange after the eruption. From product S.107f.*

A post-eruption coronal loop arcade (developing above the polarity inversion line of NOAA AR 13283) and a coronal dimming (to the northwest of NOAA AR 13283) are also visible in SDO/AIA 193Å, SDO/AIA 211 and PROBA-2/SWAP 174Å images (**Figure 7**). The arcade and the coronal dimming were indications that a coronal mass ejection (CME) was associated with this solar flare and filament eruption.

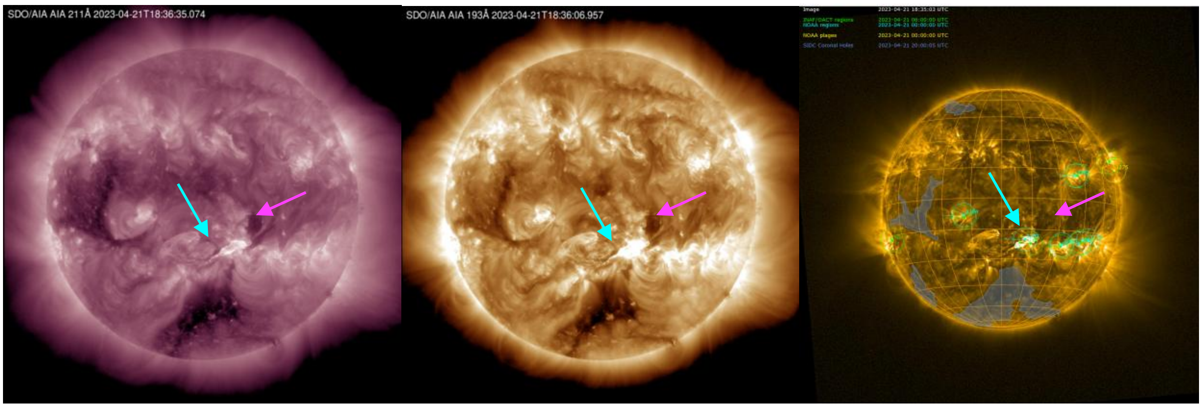

***Figure 7**: SDO/AIA 211Å (left), SDO/AIA 193Å (middle) and the SIDC Solarmap showing PROBA-2/SWAP 174 (right) images after the eruption (at 18:36 and 18:35 UTC on 21 April 2023). The post-eruptive coronal loop arcade and coronal dimming are marked in cyan and magenta, respectively. From product S.106 and S.101c, respectively.*

A full halo CME was indeed observed by coronagraphs such as SOHO/LASCO, starting at 18:12 UTC on 21 April 2023. Product S.111 (SIDC CACTus Automated near-real-time CME detection, https://swe.ssa.esa.int/sidc-S111-federated) detected a partial halo CME starting around 18:12 UTC (**Figure 8**). An alert was sent out by Product S.112b (SIDC CACTus Automated Halo CME Alert, https://swe.ssa.esa.int/sidc-S112b-federated) about 8 hours later, on 22 April at 02:22 UTC (**Figure 9**). In this alert, CACTus estimated the CME to be a partial halo (width of about 220 degrees) instead of a full halo (width of 360 degrees), but the difficulty in identifying full halo CMEs is a known limitation of CACTus. Due to the single viewpoint employed, CACTus also measured the projected speed to be around 844 km/s (ranging between 194 and 1838 km/s, across its front). The forecaster on duty at the SIDC estimated the true (de-projected) speed to be around 1100 km/s and predicted a heads-on impact at Earth between late 23 April to early 24 April (SIDC Daily space weather bulletin, https://swe.ssa.esa.int/sidc-S110-federated). Following the availability of more data over the next days, further CACTus runs continued to re-estimate the CME parameters, however although the minimum and maximum speed values changed slightly the estimated speed remained consistent around 844 km/s.

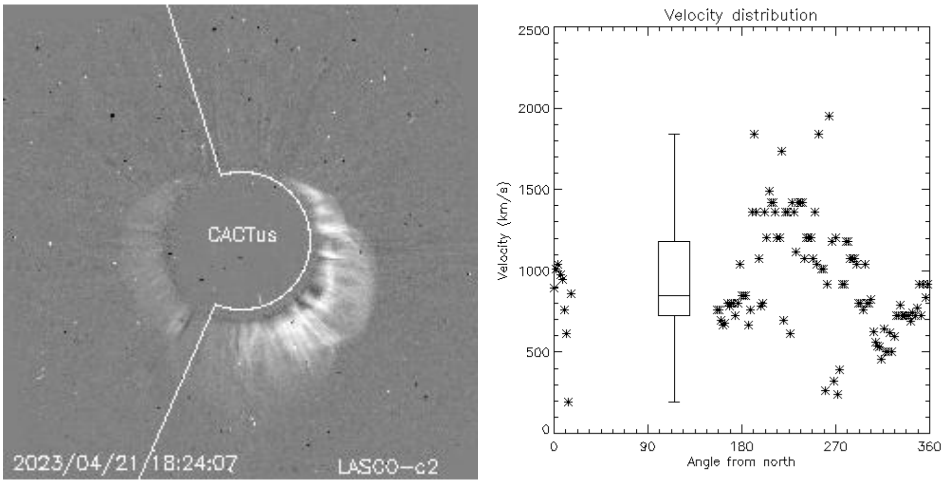

Figure 8*: SIDC CACTus automated near-real-time detection of the 21 April 2023 CME. Left: white-light image of the CME from SOHO/LASCO-C2 at 18:24 UTC, including the estimated angular width. Right: distribution of projected speeds measured along the CME front (across different position angles). From product S.111.*

issue time	alert text
2023-04-22T02:02:57.543859	A halo or partial-halo CME was detected with the following characteristics:

```
            t0        | dt0| pa  | da  |  v   |  dv  | minv| maxv|
2023-04-21T18:12:08.030 | 1.0 | 267 | 220 | 844 | 334 | 194 | 1838

       t0: onset time, earliest indication of liftoff
      dt0: duration of liftoff (hours)
       pa: principal angle, counterclockwise from North (degrees)
       da: angular width of the CME (degrees),
        v: median velocity (km/s)
       dv: variation (1 sigma) of velocity over the width of the CME
    mindv: lowest velocity detected within the CME
    maxdv: highest velocity detected within the CME
```

Figure 9*: SIDC CACTus automated alert for the 21 April 2023 CME. From product S.112b.*

In the early hours of 22 April, the UK Met Office issued the following commentary regarding this event (as provided by product H.106a, https://swe.ssa.esa.int/metoffice-alerts-e-federated):

Forecaster Guidance - 2023-04-22T01:19:34.191000
A large centre-disc full halo CME from a combination of an M1.7 flare from the vicinity of AR3283 and a filament eruption is expected to arrive at Earth at the very start of the UTC day of Monday 24 April. This may lead to Major Geomagnetic Storm G3 conditions. An earlier CME from 15 April has now most likely passed 1AU to no effect, but may pass as a small density enhancement in the coming hours. Otherwise, MOSWOC Enlil is felt to offer a reasonable assessment of conditions, but perhaps underplaying any fast wind enhancement over the current UTC weekend from CH95 (or perhaps CH94).

Forecasters at the UK Met Office also ran Enlil heliospheric simulations of the CME based on input parameters derived from GONG magnetograms and SOHO/LASCO coronagraph images. The CME input parameters used are listed in **Table 1** (where the fast Earth-directed CME observed on 21 April is highlighted) provided by product H.101a (https://swe.ssa.esa.int/metoffice-enlil-e-federated) Enlil simulation output based on inputs from **Table 1** are provided in **Figure 10**, which shows a snapshot taken around the predicted arrival time of the CME at 1 AU (around 24 April at 02:00 UTC). Similar predictions were obtained from heliospheric simulations using the EUHFORIA model (**Figure 11,** provided by product H.101g, https://swe.ssa.esa.int/ral-euhforia-e-federated), though this model forecast the CME arrival at Earth some hours later, around 24 April at 12:00 UTC. An archive of ENLIL and EUHFORIA simulations can be found in product H.113a https://swe.ssa.esa.int/ral-hparc-pb-federated .

ENLIL - CME Input Characteristics 2023-04-21T22:00:00

UTC (@ 21.5 Rs)	Longitude (deg)	Latitude (deg)	Half Width (deg)	Speed (km/s)
2023-04-15T06:56:00Z	-54	-3	21	445.0
2023-04-16T13:43:00Z	10	8	65	342.0

UTC (@ 21.5 Rs)	Longitude (deg)	Latitude (deg)	Half Width (deg)	Speed (km/s)
2023-04-17T02:45:00Z	-93	-35	26	620.0
2023-04-17T23:18:00Z	51	-58	33	418.0
2023-04-19T10:42:00Z	-56	20	23	450.0
2023-04-19T22:01:00Z	-97	-18	26	610.0
2023-04-21T12:37:00Z	83	-13	26	590.0
2023-04-21T21:21:00Z	16	-23	39	1081.0

Table 1: *CME parameters used as input to run Enlil at the UK Met Office. The fast Earth-directed CME observed on 21 April is highlighted in yellow. From product H.101a.*

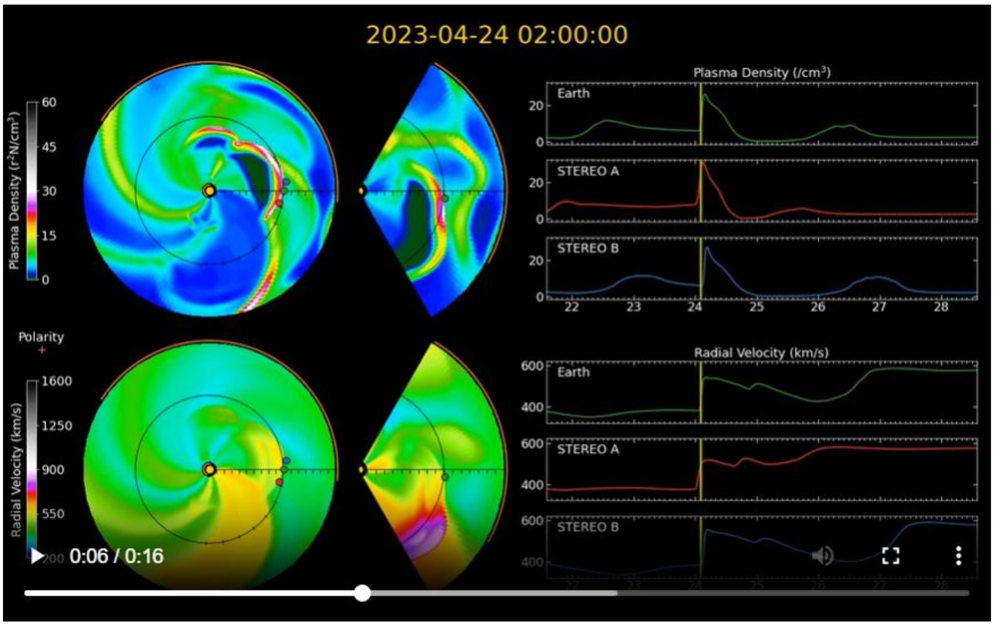

Figure 10*: Enlil outputs based on inputs from* ***Table 1****. The image shows a snapshot taken around the predicted arrival time of the CME at 1 AU (around 02:00 UTC on 24 April). From product H.101a.*

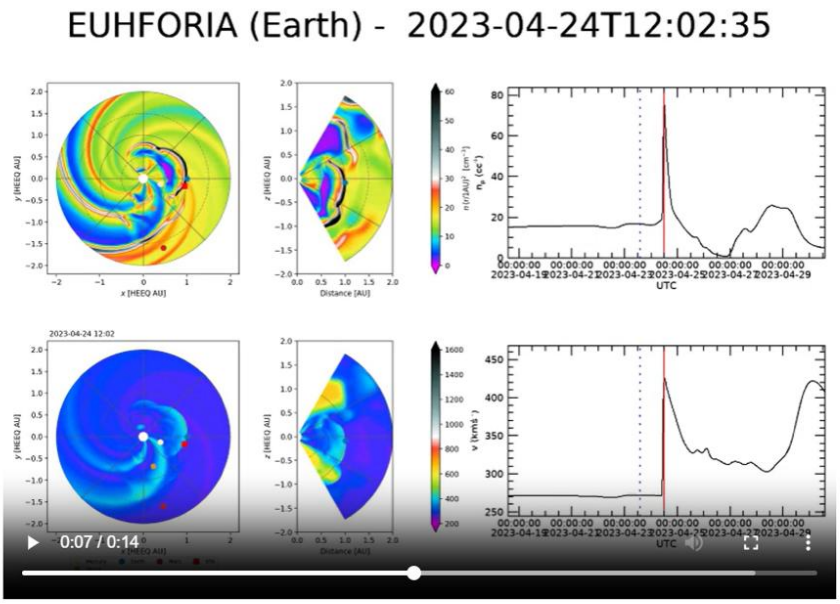

***Figure 11**: EUHFORIA outputs based on same CME inputs (see **Table 1**) used to run Enlil. The image shows a snapshot taken around the predicted arrival time of the CME at 1 AU (around 24 April at 12:00 UTC). From product H.101g. The simulations were executed by the Virtual Space Weather Modelling Centre product operated by KU Leuven (product H.200a, https://swe.ssa.esa.int/kul-cmpa-federated).*

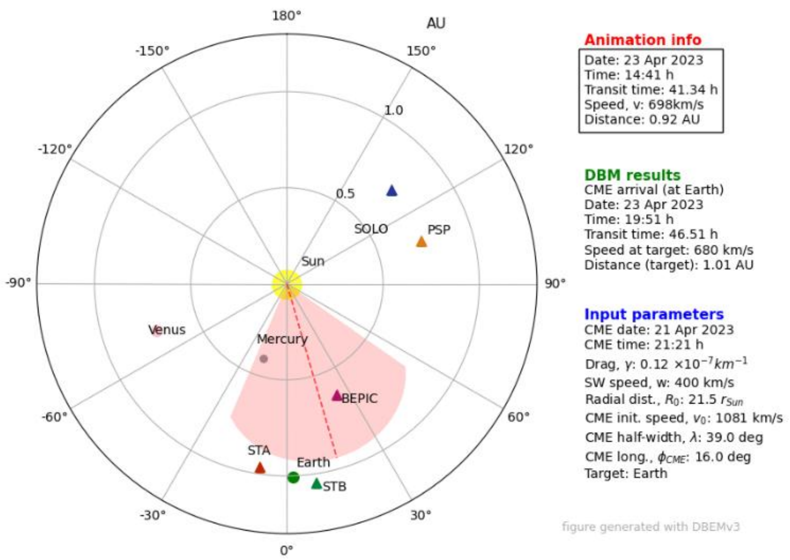

***Figure 12**: UNIGRAZ/IGAM DBEM output based on same CME inputs (see **Table 1**) as Enlil and EUHFORIA simulations. The image is of the predicted progression of the CME at the stated time. The model was run at ~08:30 UTC on the 22nd. (predicted on 23 April at 19:51 UTC). From product H.108b.*

Additional predictions of the CME arrival time were obtained from the Drag-Based Ensemble Model (DBEM), available through product H.108b (https://swe.ssa.esa.int/graz-dbem-federated). The detailed DBEM predictions, based on the CME input parameters in **Table 1**, is shown in **Figures 12** and **13**. This model predicted the CME arrival time at Earth on 23 April at 19:51 UTC (**Figure 12)**. When uncertainties in the solar wind and CME input parameters were used to define the ensemble parameter space, the forecast window for the

CME arrival time ranged from 23 April at 12:07 UTC to 24 April at 08:12 UTC (**Figure 13**). . The archive for the ENLIL movies and DBEM runs can be found in the product H.112a (https://swe.ssa.esa.int/ral-hparc-par-federated). Overall, the CME was predicted to arrive at Earth at the very start of the UTC day of 24 April, and was expected to lead to Strong Geomagnetic Storm G3 (Kp=7) conditions (based on NOAA SWPC Storm Scales, https://www.swpc.noaa.gov/noaa-scales-explanation).

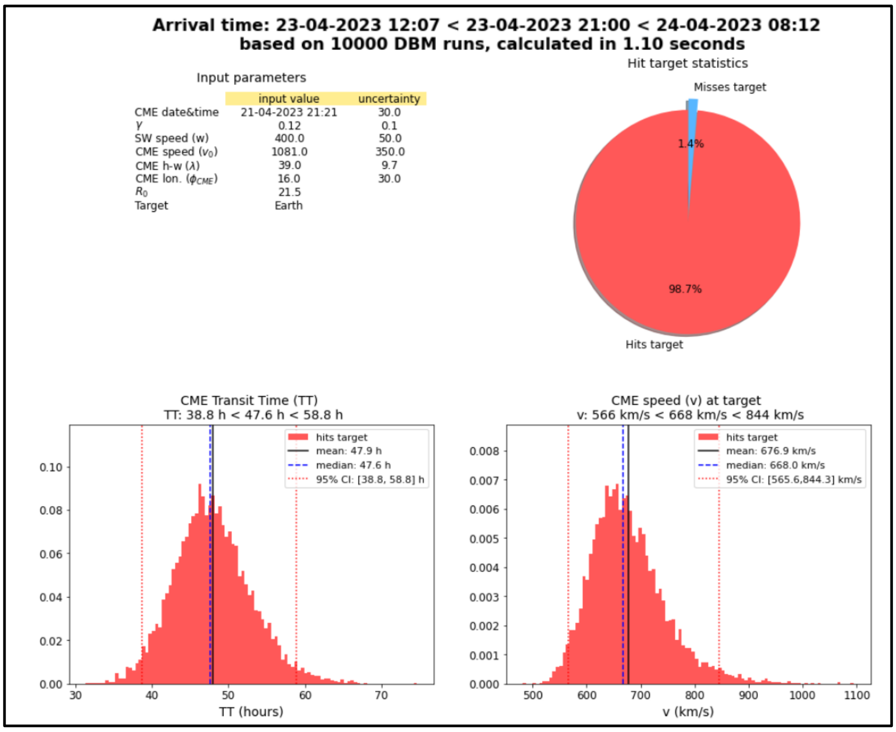

***Figure 13**: UNIGRAZ/IGAM DBEM output based on same CME inputs (see **Table 1**) as Enlil and EU-HFORIA simulations. The image shows the details of the DBEM output predictions at Earth, based on 10,000 ensemble members. From product H.108b.*

The STEREO-A spacecraft was close to the Earth at this time (trailing by about 10 degrees in longitude) and as such did not have a good side on view of this CME. A weak trace was visible in the Heliospheric Imager time elongation plots from the spacecraft NRT (Beacon mode) data. The annotated version provided with overplotted drag based model profile (product H.120c) indicated that signature was consistent the DBM forecast.

The arrival of the CME at Earth (DSCOVR) and STEREO-A was captured by DTU's AWARE automated detection of CME arrival and interplanetary shock (**Figure 14**, from products H.106b https://swe.ssa.esa.int/dtu-aware-federated and H.110b https://swe.ssa.esa.int/dtu-aware-a-federated) based on DSCOVR and STEREO-A data. At DSCOVR, the interplanetary shock arrived on 23 April at 16:59 UTC (i.e. about 10 hours before predicted by Enlil simulations), while it arrived at 14:28 UTC at STEREO-A. DTU's AWARE product correctly detected the shock at 16:59 but did indicate the start of the ICME period earlier (around 07:00 UTC and 04:00 UTC, before the shock arrivals), possibly due to the use of beacon's data and the presence of data gaps and issues with the plasma data, forcing the detection methods to rely only on magnetic field data (particularly in the case of STEREO-A). The near-real-time prediction of the Kp index from DTU at Earth (**Figure 14**, top left) shows that the Kp index was predicted to reach a value of 7 (Geomagnetic Storm Scale G3 - Strong) immediately after the shock passage. This prediction was thus consistent with the prediction mentioned in the initial commentary issued by the UK MET Office and reported above. The arrival of the CME structure was also confirmed by the INAF MagEffTool (**Figure 14**, bottom). The MagEffTool is based on the quantification of the magnetic helicity spectrum and integrated spectrum (**Figure 14,** bottom figure, lower two panels) derived from insitu observations of the IMF at L1. A strong signal was observed in the short scale helicity at around 18:00 UTC consistent with the arrival and passage of the CME determined with AWARE.

Figure 15 (from product H.101z, https://swe.ssa.esa.int/ral-swfsc-e-federated) shows the comparison between the observed solar wind speed at L1, and a number of solar wind forecasts (including Enlil and ESWF24), among other solar wind speed forecasts. The in-situ arrival of the interplanetary shock associated with the CME fits quite well with the DBEM-based predicted CME arrival window from **Figure 13**, while Enlil predictions are about 4 hours late compared to observations. Note that ESWF24 (UNIGRAZ/IGAM's forecast of solar wind high-speed streams from product H.101h, https://swe.ssa.esa.int/graz-eswf24-federated) is only a background solar wind forecast and therefore the enhancement seen towards the end of 24 April is not real (it appears because the model is responding to the solar wind enhancement caused by the interplanetary CME on 23 April).

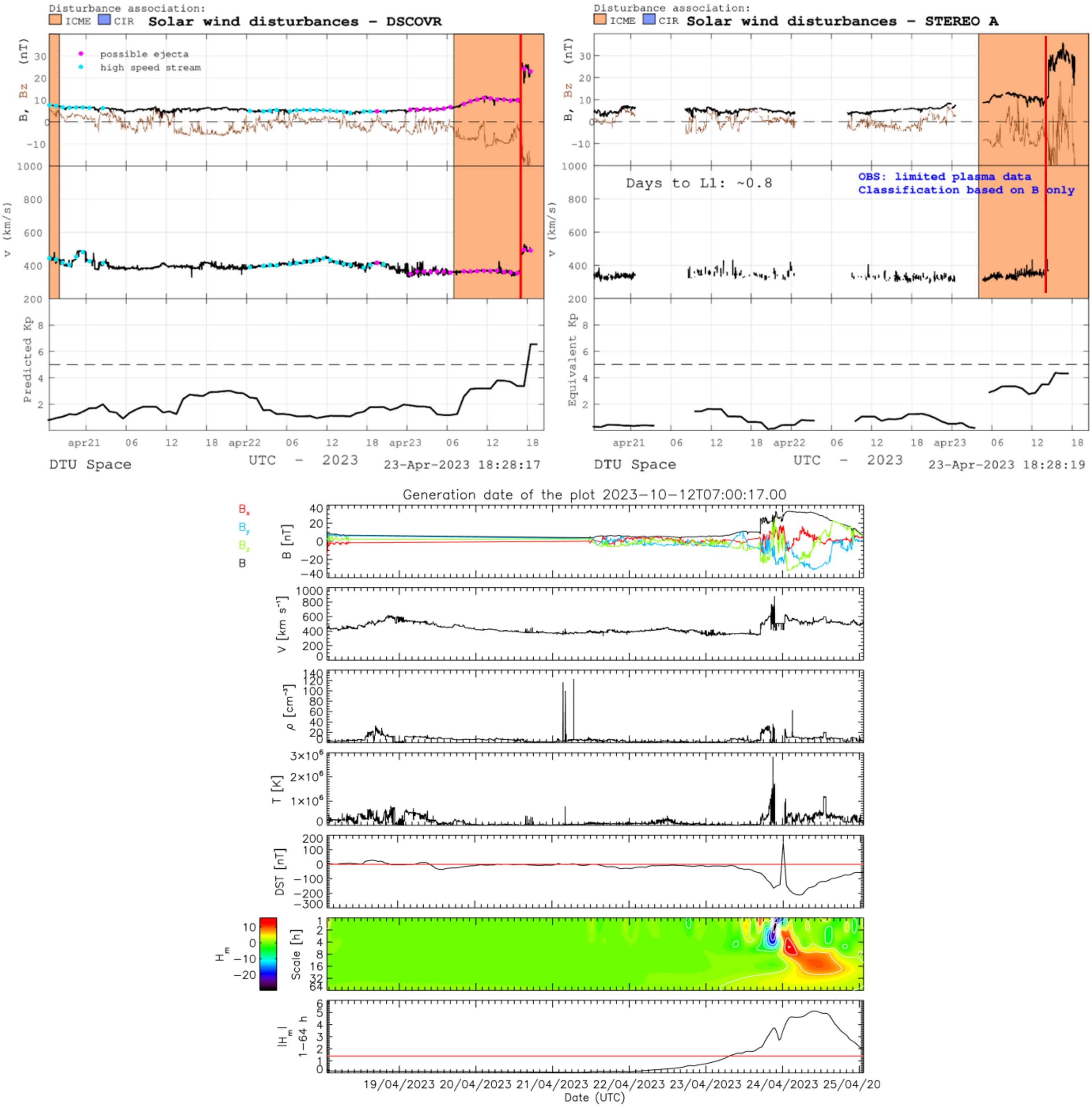

***Figure 14**: DTU's AWARE automated detection of the CME arrival at Earth (top left) and STEREO-A (top right). The interplanetary shock arrivals are marked by the red vertical lines, while the magnetic ejecta periods are marked by the shaded orange regions. The bottom panels show the near-real-time predictions of the Kp index. From products H.106b (top left) and H.110b (top right). INAF Magnetic Effectiveness Tool (bottom) showing the magnetic helicity computed from the IMF measured by DSCOVR. From product H.103d.*

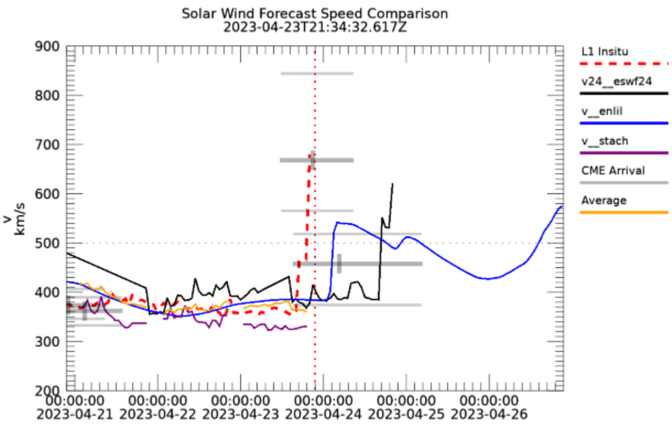

***Figure 15**: Comparison of solar wind model forecast and actual L1 observations from RAL/STFC. The comparison is performed at 21:34 UTC on 23 April. From product H.101z.*

On 24 April, following the CME arrival at Earth, the UK Met Office issued the following commentary (as provided by product H.106a, https://swe.ssa.esa.int/metoffice-alerts-e-federated):

> Forecaster Guidance - 2023-04-24T13:45:58.441000
> A large centre-disc full halo CME arrived at Earth at 23/1730 UTC, on the leading edge of the ENLIL ensemble spread. Geomagnetic activity increased to G3-G4 Strong to Severe Storm conditions. Solar winds reached 700-800 km/s, again closer to the faster ENLIL ensemble members. Activity now beginning to wane, though CME influence forecast to continue into the 25th. Strong signal for arrival of HSS and potential CIR associated with CH96/- later on the 26th into the 27th accepted.

By the time this second commentary was issued, the geomagnetic activity had thus exceeded the initial forecast of G3 (Strong, Kp=7) storm level as it had quickly reached a G4 (Severe, Kp=8+) storm level. This was driven by the passage of the interplanetary CME-driven shock, which was characterized by a strong dynamic pressure and prolonged negative IMF Bz.

The intense geomagnetic activity associated with this space weather event, both locally and globally, was extensively captured by the network**.** Magnetograms of the horizontal intensity (H) of the magnetic field in North(West) Europe and Greenland on 23-24 April illustrate the very active magnetic field across that region (as shown in **Figure 16**, from product G.101: https://swe.ssa.esa.int/nrt-mag-federated). The magnetometers that generate the magnetograms are monitored by several institutes and cover a large region both in longitude and latitude. **Figure 17** shows the first derivative of the horizontal intensity of the magnetic field, dH/dt, in units of nT/s, from magnetometer stations distributed between 54 and 84 degrees in magnetic latitude (as provided by product G.159, https://swe.ssa.esa.int/dMAG_dt-federated). Large amplitudes of several hundreds of nTs in the horizontal intensity can be seen, especially between 12:00 UTC on 23 April and 12:00 UTC on 24 April. Large variations in the horizontal component of the magnetic field, dH/dt, are also prominent in the periods between approximately 17:30 UTC to 22:00 UTC on 23 April, and between approximately 01:00 UTC – 07:00 UTC at sub-auroral latitudes, 03:00 UTC – 13:00 UTC at auroral latitudes and 09:00 UTC – 14:00 UTC at higher latitudes (UPN) on 24 April. The most intense and rapid variations are seen at 19:00 UTC – 21:00 UTC on 23 April in the Faroe Islands (HOV) and Narsarsuaq, Greenland (NAQ), at 03:00 UTC – 07:00 UTC on 24 April in HOV, and at 03:00 UTC – 10:00 UTC on 24 April in NAQ. The local K-index recorded by the magnetic ground stations in Brorfelde (BFE) and Dombås (DOB) is shown in **Figure 18** (provided by product G.102, https://swe.ssa.esa.int/dtu-k-federated) for 23 and 24 April. As can be seen, at both locations the local K-index was as high as 5 or above in the whole period between 15:00 UTC on 23 April and 09:00 UTC on 24 April. At BFE, the local K-index reached a maximum value of 8 at 18:00 UTC – 21:00 UTC on 23 April and 03:00 UTC – 06:00 UTC on 24 April. At DOB, the local K-index reached values of 9 at 18:00 UTC – 21:00 UTC on 23 April and 00:00 UTC – 09:00 UTC on 24 April.

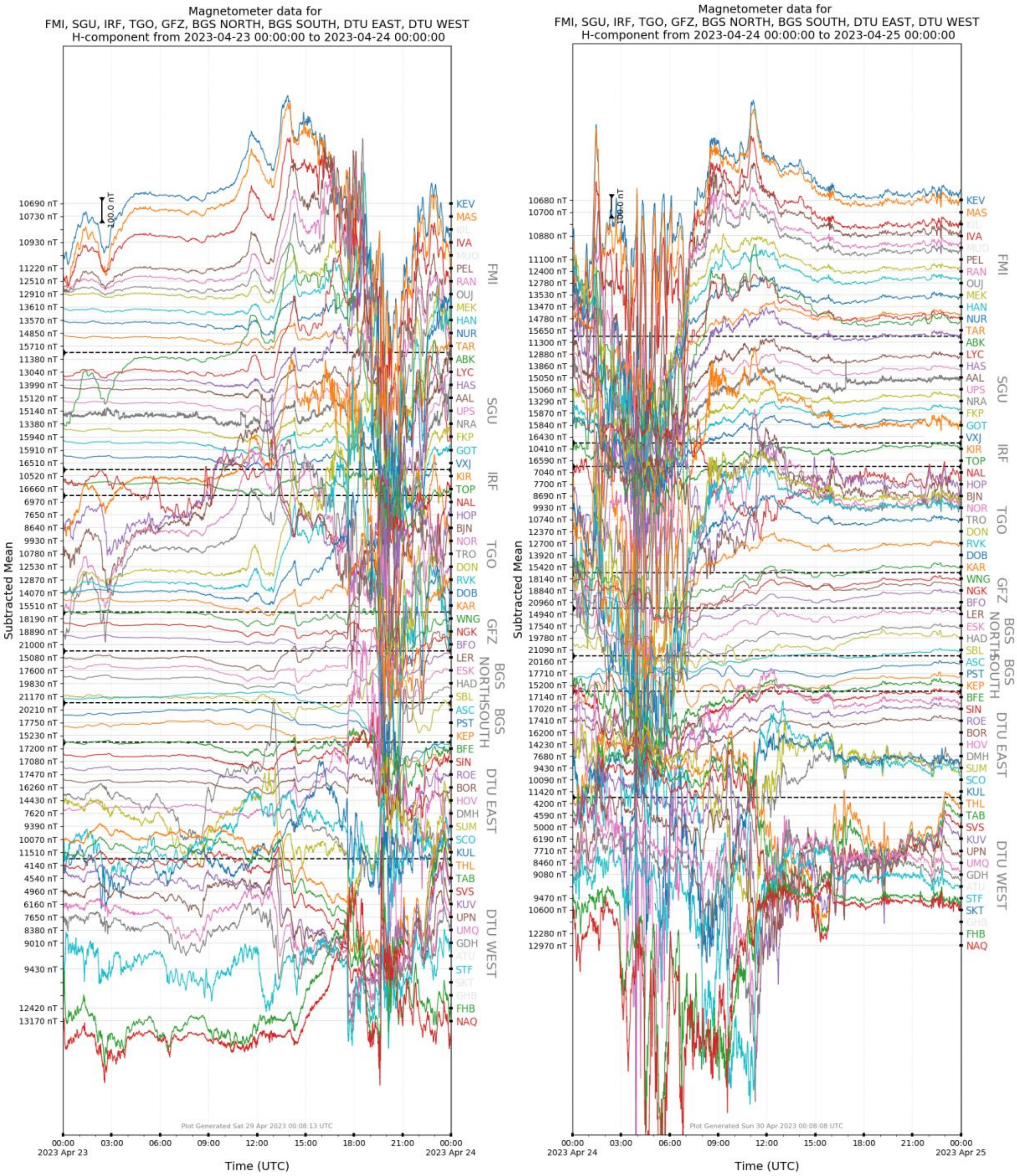

Figure 16: *Magnetograms from North(West) Europe and Greenland. From product G.101.*

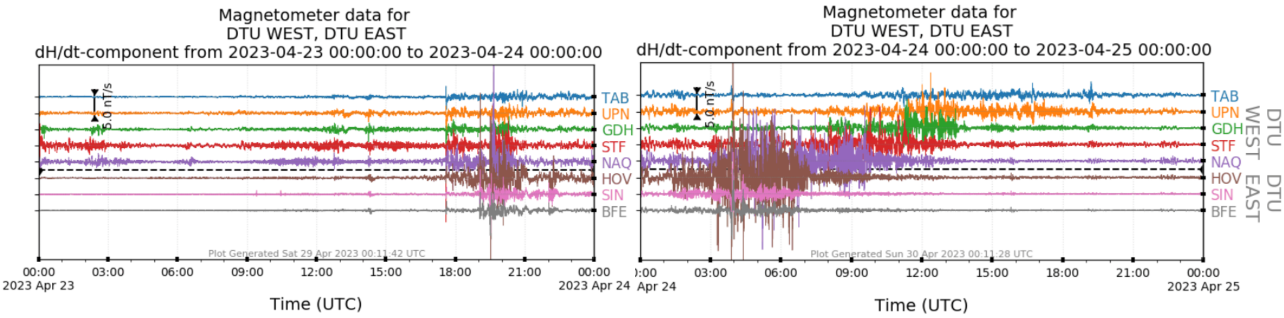

***Figure 17**: DTU GIC indicator plots for Greenland and Northern Europe for 23 April (left) and 24 April (right). From product G.159.*

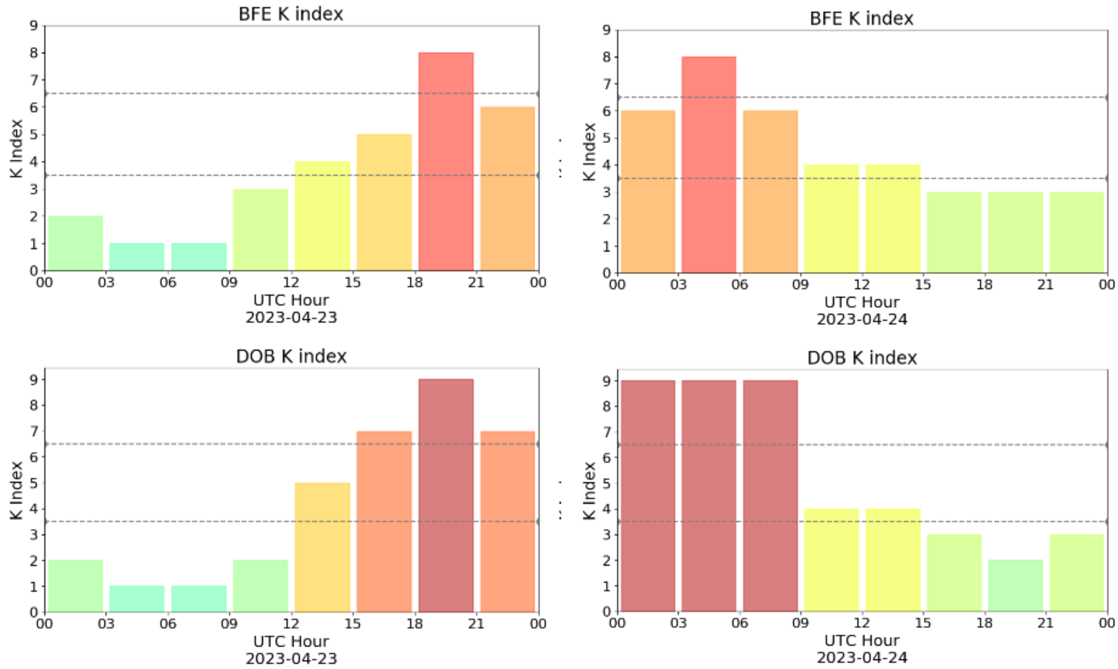

***Figure 18:** Local K-index from magnetometer stations in Brorfelde (BFE, top) and Dombås (DOB, bottom) in Northern Europe, for 23 April (left) and 24 April (right). From product G.102.*

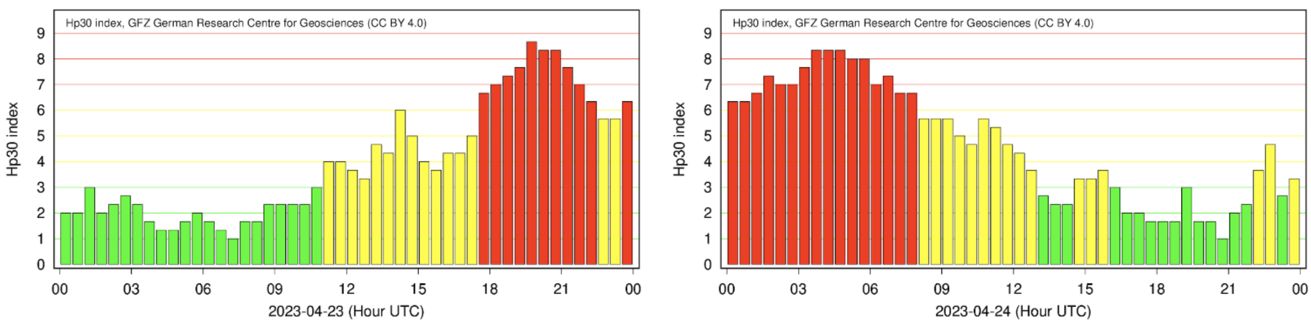

***Figure 19:** Global Hp30 index, for 23 April (left) and 24 April (right). From product G.154a*

Globally, the real-time Hp30 index, an open-ended Kp-like 30-minute index by GFZ (see **Figure 19**, data from the providor's own archive) indicate that the geomagnetic storm started developing around 17:30 UTC on 23 April as a consequence of the negative Bz values in the IMF (shown in **Figure 22**, second panel, note that the Kp index by GFZ is shown in red in the top panels). After the arrival of the CME-driven shock at 16:59 UTC on 23 April (at DSCOVR, in **Figure 14**), the Kp values continued to increase in response to the intense solar wind dynamic pressure (controlled by the solar wind density and speed) and strong negative IMF Bz values. The maximum Kp value of 8+ was reached at 18:00 – 21:00 UTC on 23 April and 03:00 – 06:00 UTC on 24 April. The top panel in **Figure 22** (blue bars) also displays the forecast Kp from IRF for the period 21-26 April (from product G.134, https://swe.ssa.esa.int/irf-federated). In this case, Kp predictions made by IRF with a few hours of lead time were consistent with Kp observations, with differences never exceeding +/- 1. **Figure 23** displays the forecast Dst from IRF (blue bars) and the real-time Dst from Kyoto (red bars) (from product G.135, https://swe.ssa.esa.int/irf-federated). The Dst index followed a similar (mirrored) behaviour as the Kp index, and reached its minimum value of -212 nT at 18:00 – 19:00 UTC on 23 April, just before the IMF Bz turned from negative to positive values (as shown in **Figure 14,** left). Dst predictions made by IRF were overall consistent with Dst observations for 23 April, with differences never exceeding +/- 25 nT. However, on 24 April the Dst was significantly under-predicted compared to measured values, with forecasts reaching -100 nT compared to observations.

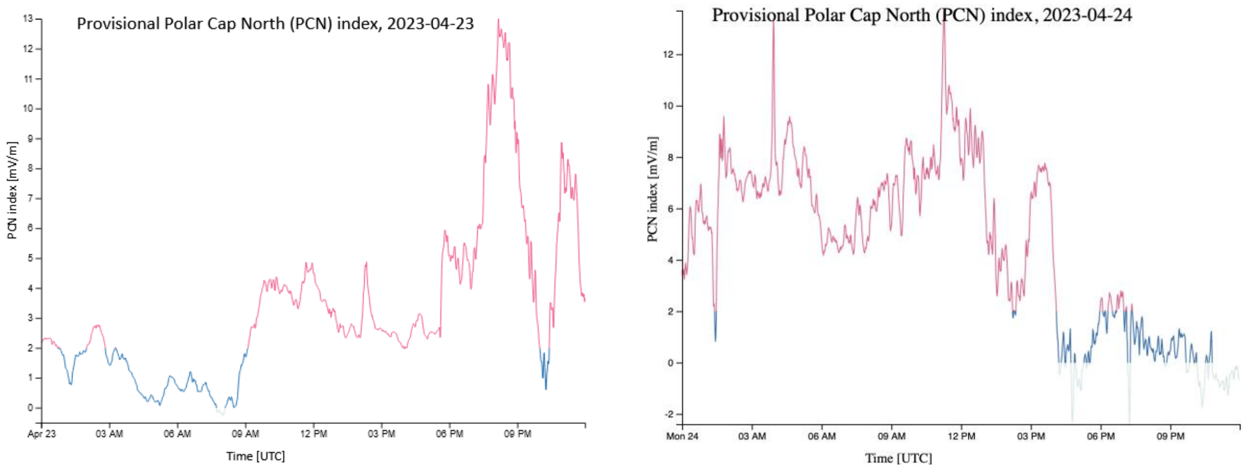

Figure 20. *PCN index. PCN index values above 2 mV/m are shown in magenta. From product G.144.*

The Polar Cap North index (PCN index) monitors the energy input from the solar wind to the magnetosphere (loading activity). The index is constructed as a linear relationship with the merging Electric Field at the magnetopause. During quiet conditions, the index is close to 0 mV/m, and statistical studies has shown that the index only exceeds 2 mV/m in 20% of the time. **Figure 20** shows provisional plots of the PCN index on 23 April (left) and 24 April (right) from product G.144 (https://swe.ssa.esa.int/dtu-pcn-federated). The PCN index was above 2 mV/m (in magenta) for almost the entire period between 9:00 UTC on 23 April and 16:00 UTC on 24 April. PCN values over 10 mV/m are extremely rare (more information on the distribution of the PCN index values is illustrated in figure ***Figure 21***) , but are seen both on 23 April and 24 April.

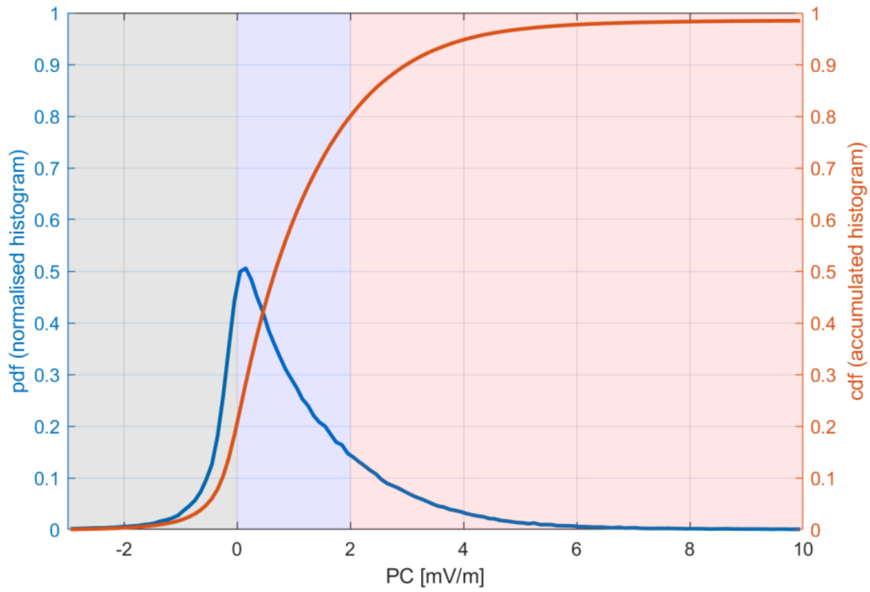

Figure 21: *The figure shows the distribution of the PCN index as a probability density function (pdf) estimate and a cumulative density function (cdf) estimate. Note that the x-axis is fixed between -3 and 10mV/m in this figure.*

Figure 24 shows the forecast for the AE (top), AU and AL (bottom) indices (from product G.145, https://swe.ssa.esa.int/irf-federated). These indices are some of the few fundamental and IAGA endorsed geomagnetic indices, that provide an indication of the electrojet intensity.

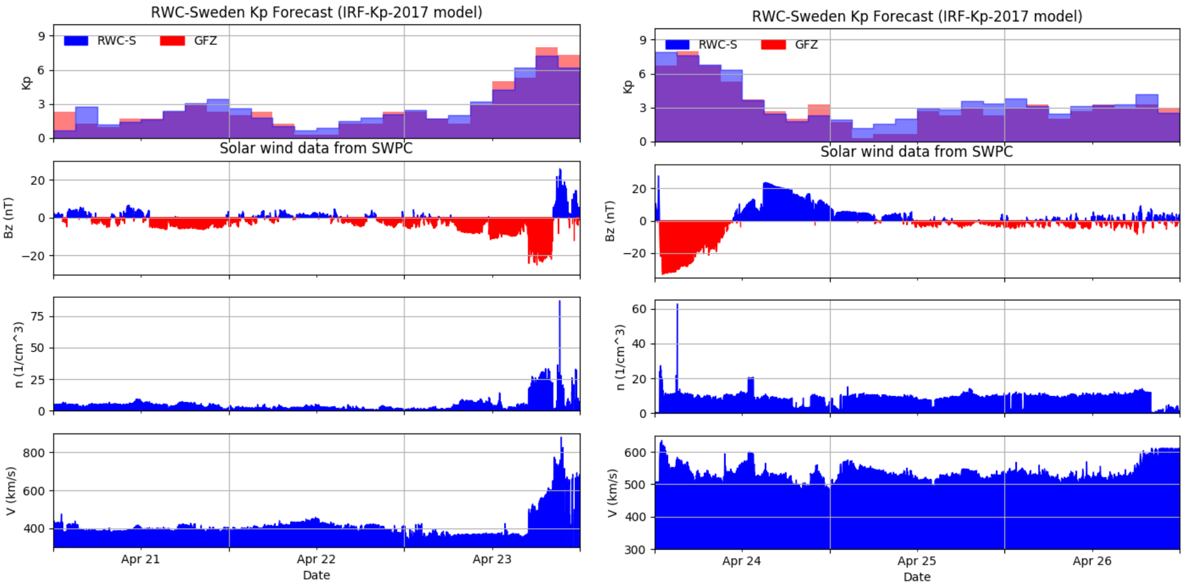

Figure 22*: In the top panel of the graphs is a forecast Kp from IRF (in blue) and measured Kp from GFZ Potsdam (in red), for the period 21-26 April. Each Kp bar has a width of 3 hours. As the model uses data from L1 the Kp forecast lead time is between 1 and 4 hours. The three bottom panels show the solar wind conditions (IMF Bz, solar wind number density and solar wind speed) from NOAA SWPC. Note the different y-axis scales in the left and right panels. From product G.134.*

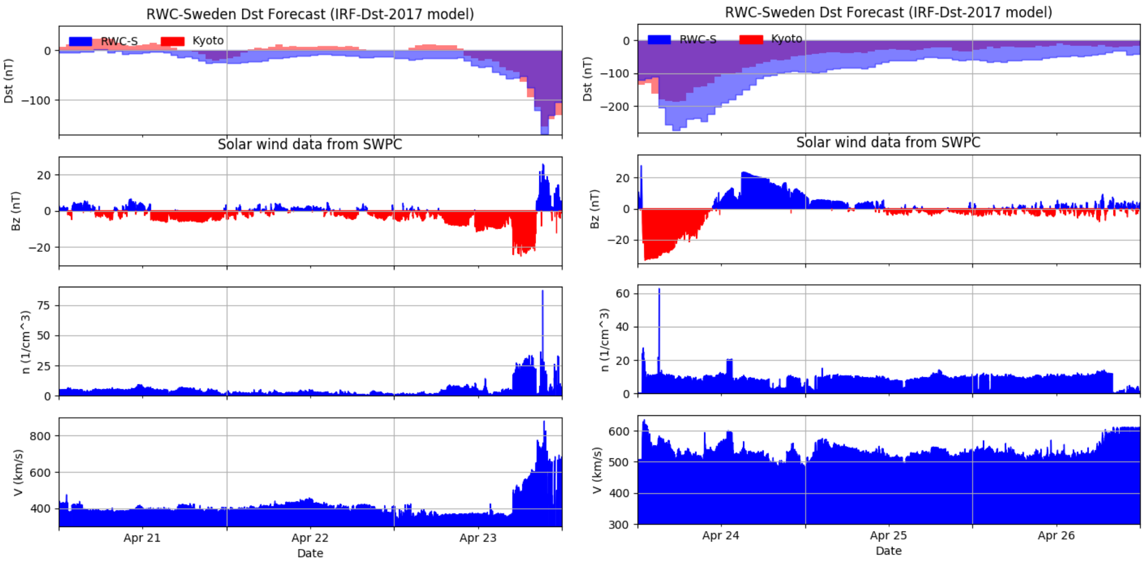

Figure 23: *In the top panel of the graphs is a forecast Dst from IRF (in blue) and measured Dst from Kyoto (in red), for the period 21-26 April. Each bar has a width of 1 hour. As the model uses data from L1 the Dst forecast lead time is typically less than 2 hours. The three bottom panels show the solar wind conditions (IMF Bz, solar wind number density and solar wind speed) from NOAA SWPC. Note the different y-axis scales in the left and right panels. From product G.135.*

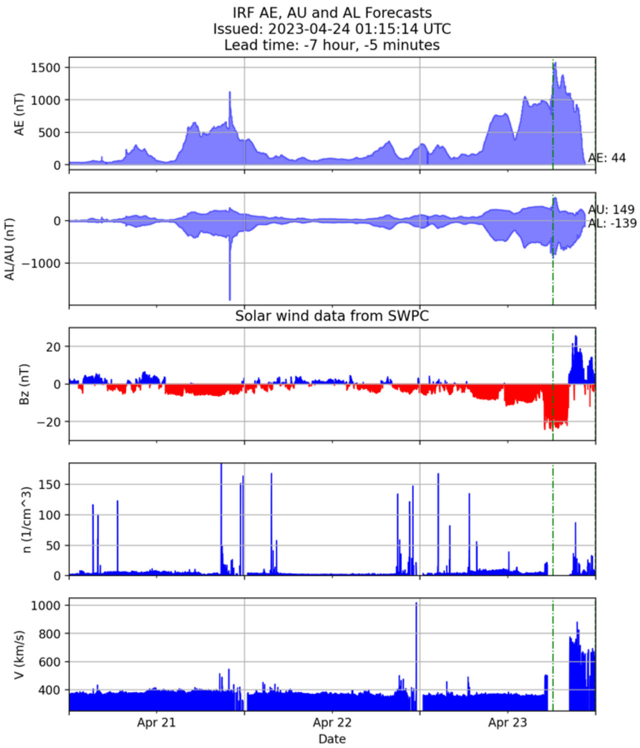

Figure 24: *Forecast of AE, AU and AL indices for the period 21-23 April. Each bar has a width of 5 minutes. The three bottom panels show the solar wind conditions (IMF Bz, solar wind number density and solar wind speed) from NOAA SWPC. Values for the latest AE, AU and AL forecasts are shown after the last bar. The timestamp of the latest predicted value is shown with the dash-dotted line. From product G.145.*

Starting from around noon (UTC) on 23 April, the radiation environment at L1 and GEO was also affected by the approaching interplanetary CME. A drop-out electron event, corresponding to a decrease in the omni-directional Differential Electron Flux (FEDO) from EDRS-C/NGRM L2 data at GEO, was observed between 12:00 UTC con 23 April and 12:00 UTC on 24 April (as shown in **Figure 25**, provided by product R.170 (https://swe.ssa.esa.int/sparc-geo-ngrm-r170-federated). Around the same time, a solar proton event (SPE) was ongoing and visible as an increase in the omni-directional Differential Proton Flux (FPDO) in EDRS-C/NGRM L2 data at GEO, provided by product R.171 (https://swe.ssa.esa.int/sparc-geo-ngrm-r171-federated), as shown in **Figure 26**.

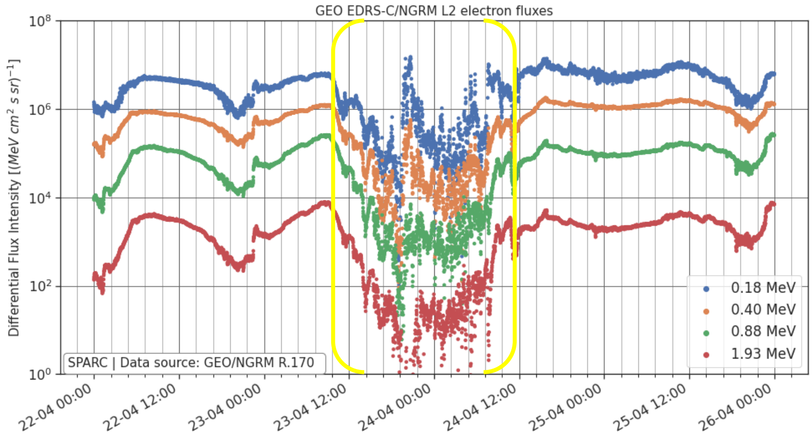

***Figure 25**: EDRS-C/NGRM L2 electron differential fluxes (FEDO) at GEO on 22-26 April 2023. The drop-out electron event is highlighted in the yellow box. From product R.170.*

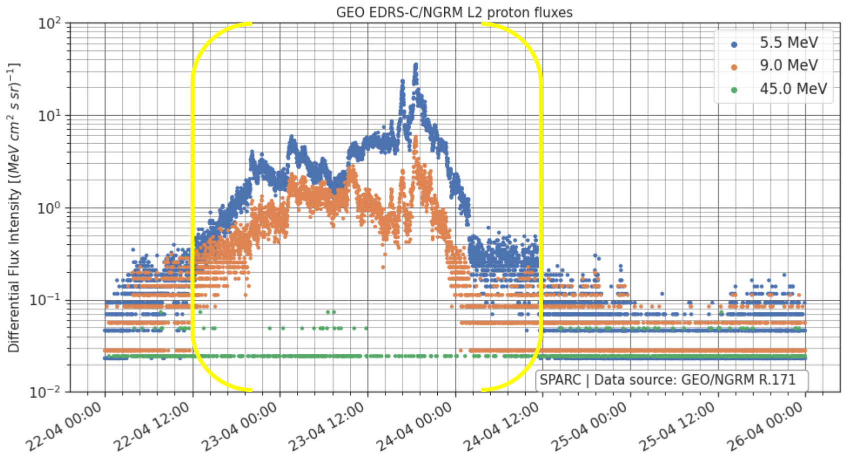

***Figure 26:** EDRS-C/NGRM L2 proton differential fluxes (FPDO) at GEO on 22-26 April 2023. The SPE is highlighted in the yellow box. From product R.171.*

Increases in the SOHO/COSTEP/EPHIN proton and electron fluxes measured at L1 were observed around 17:30 UTC on 23 April 2023 (**Figure 27**, top and bottom panels). Specifically, electron event onsets (indicated in magenta) were observed at 16:58 UTC and 17:25 UTC, whereas the real-time proton flux was observed to increase at 17:44 UTC in the 30 – 50 MeV energy range. A comparison with observations at ACE is unfortunately not possible due to a data gap affecting the ACE/EPAM EPHIN real-time electron flux data during these increases (**Figure 28**, bottom panel). HESPERIA REleASE real-time forecasts issued on 23 April and based on SOHO/COSTEP/EPHIN and ACE/EPAM EPHIN real-time electron flux data are shown in **Figures 27** and **28** (as provided by product R.158, https://swe.ssa.esa.int/noa-hesperia-federated). **Figure 27** (shows that the HESPERIA REleASE alert product generated a proton intensity alert level at 17:30 UTC on 23 April. Therefore, an advanced-warning-time (AWT) of about 15 minutes was provided for this particular event. It is noteworthy that the nominal AWT for most of the events is greater than 60 minutes. **Figure 28** shows that there was a gap in the measured ACE/EPAM EPHIN real-time electron flux data during the occurrence of this increase, so it was not possible to provide a forecast based on these data.

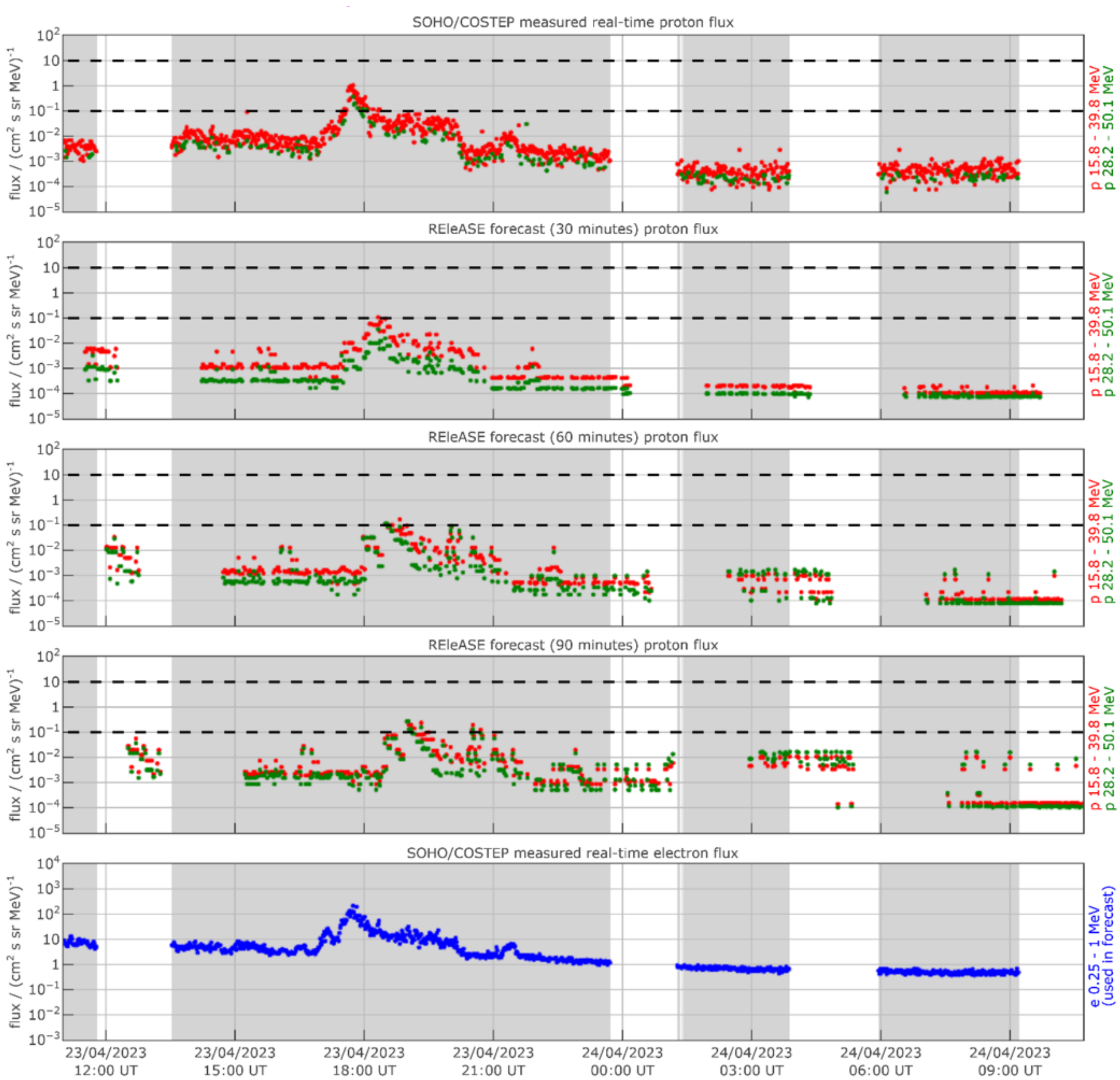

Figure 27: *The 23 April 2023 real-time forecast results based on SOHO/COSTEP/EPHIN real-time electron flux data taken at L1. Top panel: real-time proton fluxes measured by SOHO/COSTEP/EPHIN. Next three panels: SOHO/COSTEP/EPHIN proton flux forecasts. The forecasts are shown shifted in time by 30, 60 and 90 minutes, respectively. Bottom panel: measured SOHO/COSTEP/EPHIN real-time electron flux at 0.25 - 1 MeV energy, used for the forecasts. Magenta arrows mark electron and proton event onsets. From product R.158.*

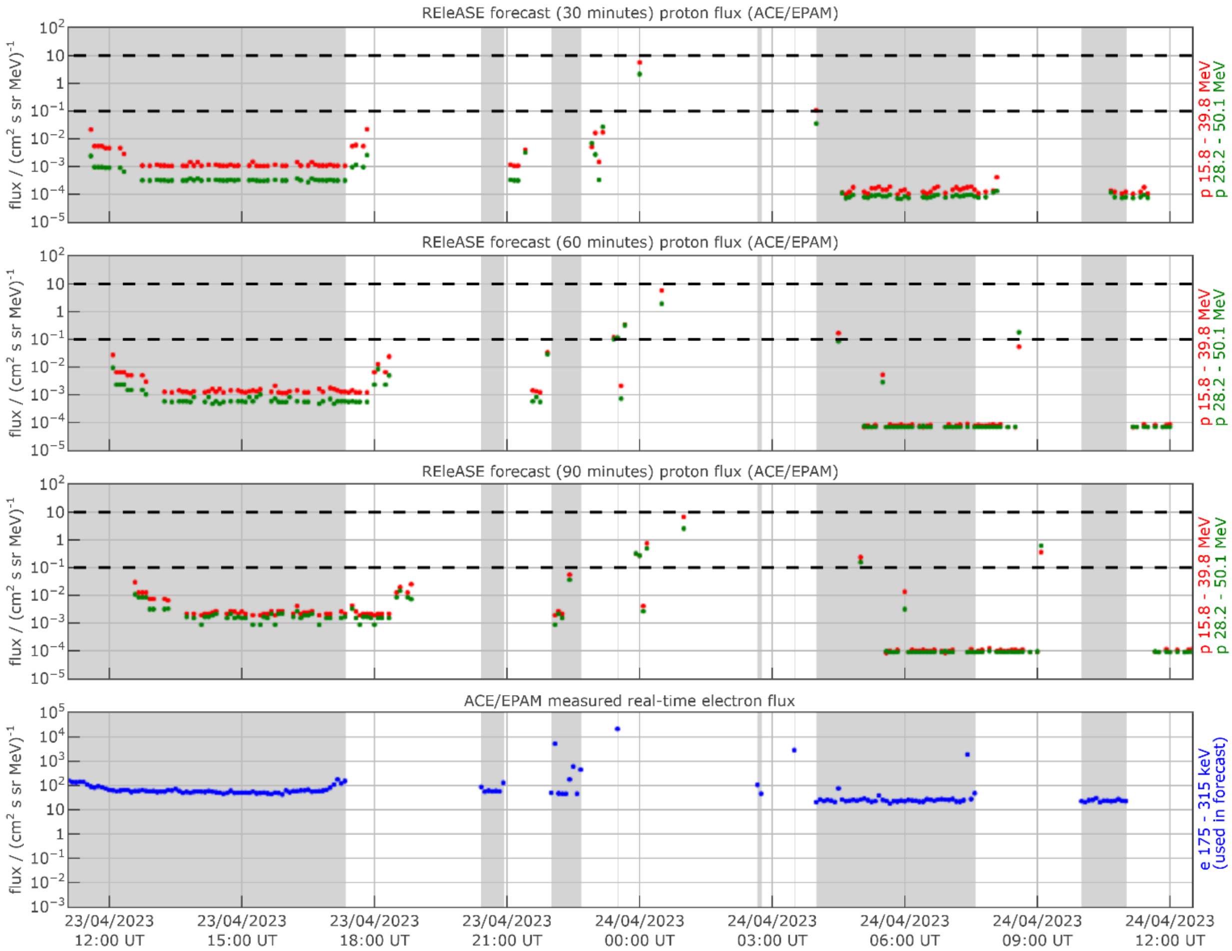

Figure 28: *The 23 April 2023 real-time forecast results based on ACE/EPAM EPHIN real-time electron flux data taken at L1. First three panels: ACE/EPAM real-time proton flux forecasts. The forecasts are shown shifted in time by 30, 60 and 90 minutes, respectively. Bottom panel: measured ACE/EPAM EPHIN real-time electron flux at energy of 0.175 - 0.315 MeV, used for the forecasts. From product R.158.*

The ionospheric environment and telecommunication systems relying on wave propagation through the ionosphere, were also affected by this space weather event. A depletion of the Total Electron Content (TEC) was observed at high latitudes (>50° N) from 23 April at 18:00 UTC, as shown by the Near-real time TEC maps over Europe in **Figure 29** (provided by product I.101b by DLR/IMPC, https://swe.ssa.esa.int/impc-federated**)**. Looking at the contour lines in **Figure 29**, there is a consistent increase of around 5 to 10 TECU when comparing the TEC maps from the 23rd to the 24th, which is a significant increase. A strong impact on GNSS across Norway was also observed between 18:00 UTC on 23 April and 09:00 UTC on 24 April, as shown in the Rate of TEC Index (ROTI) at ground time series and maps on Fennoscandia (I.109b ROTI@Ground maps -Fennoscandia) **Figure 30** (provided by product I.109b, https://swe.ssa.esa.int/rtim-federated). Vertical TEC (VTEC) time series also showed unusual TEC values over Northern Europe in the evening (UTC) of 23 April, and suppressed TEC levels in the early UTC hours on 24 April (**Figure 31**, provided by product I.107, https://swe.ssa.esa.int/rtim-federated). Maps of the scintillation index σφ in **Figure 32** indicate increased scintillation for L1 frequency over Norway in the UTC evening of 23 April (provided by product I.110b, https://swe.ssa.esa.int/rtim-federated). NOA EIS nowcasting foF2 maps at 20:00-21:00 UTC on 23 April also show that negative storm effects were detected all over Europe, as predicted by the SWIF model (**Figure 33**, from product I.115, https://swe.ssa.esa.int/dias-federated).

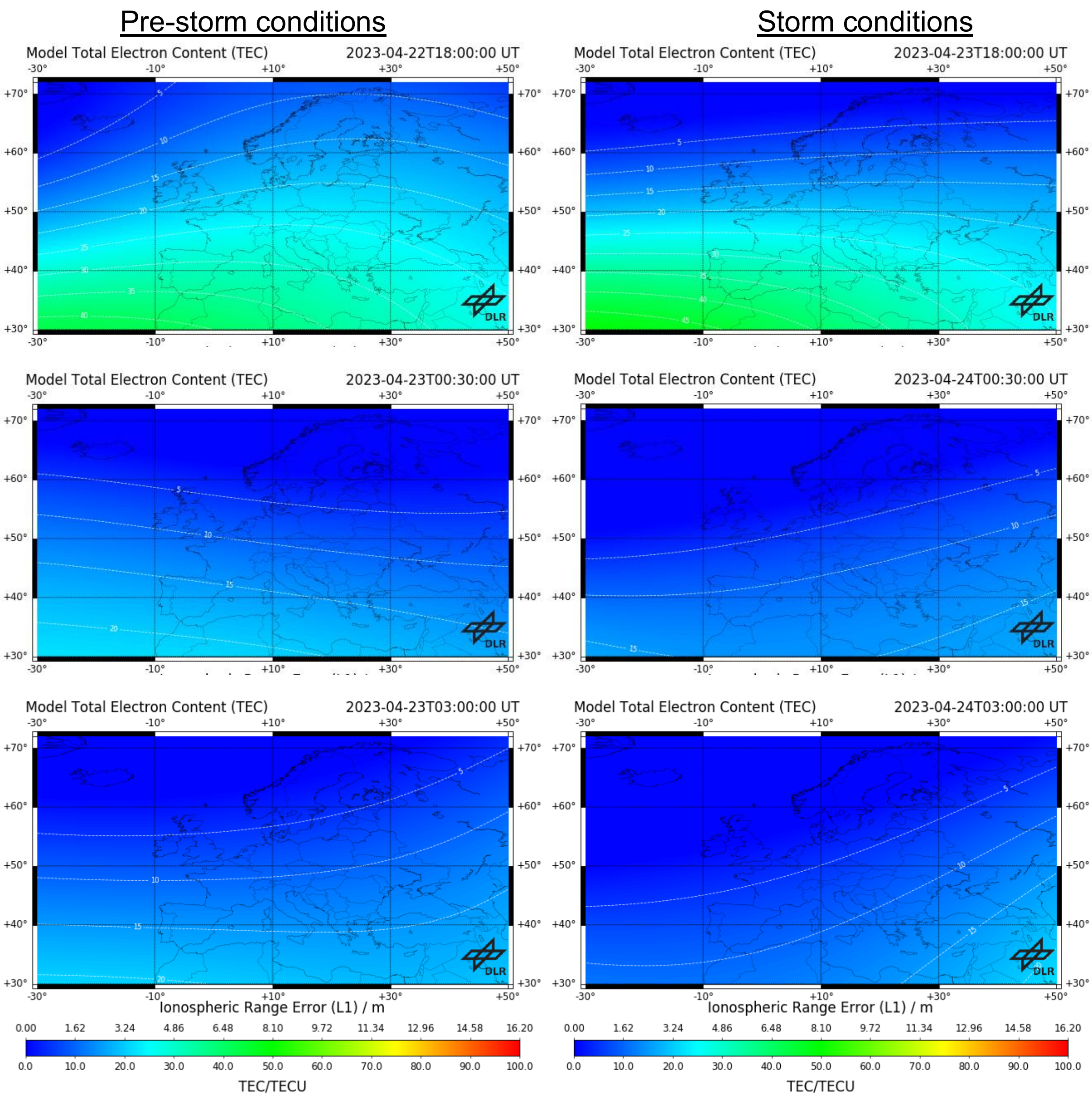

Figure 29*: DLR/IMPC TEC Maps for Europe between 22 and 24 April. From product I.101b.*

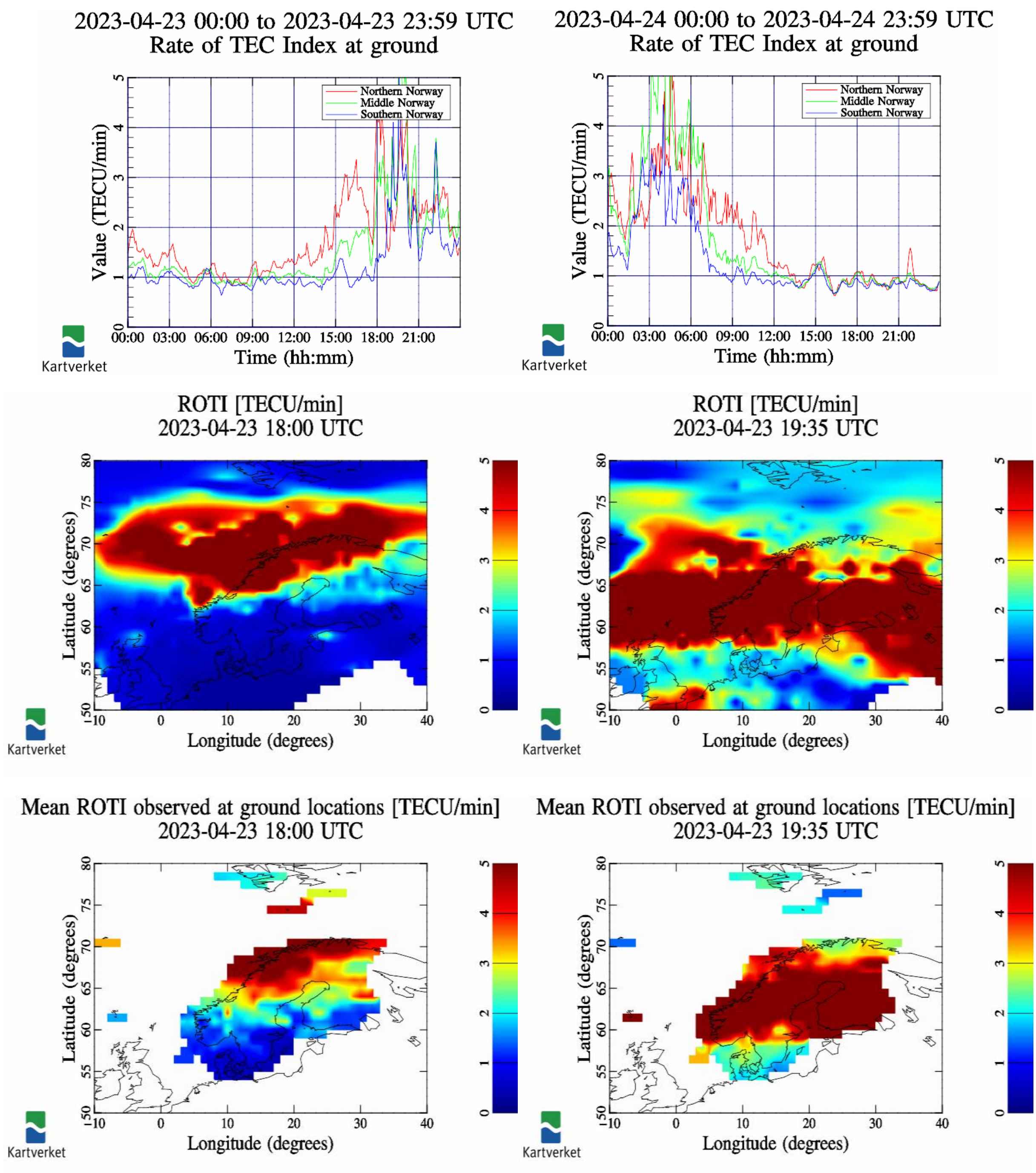

Figure 30*: NMA ROTI@Ground conditions (Fennoscandia) on 23 April and 24 April. Top: ROTI@Ground time series for Norway on 23 April and 24 April. Middle and bottom: ROTI and mean ROTI at ground maps in the evening of 23 April. From product I.109b.*

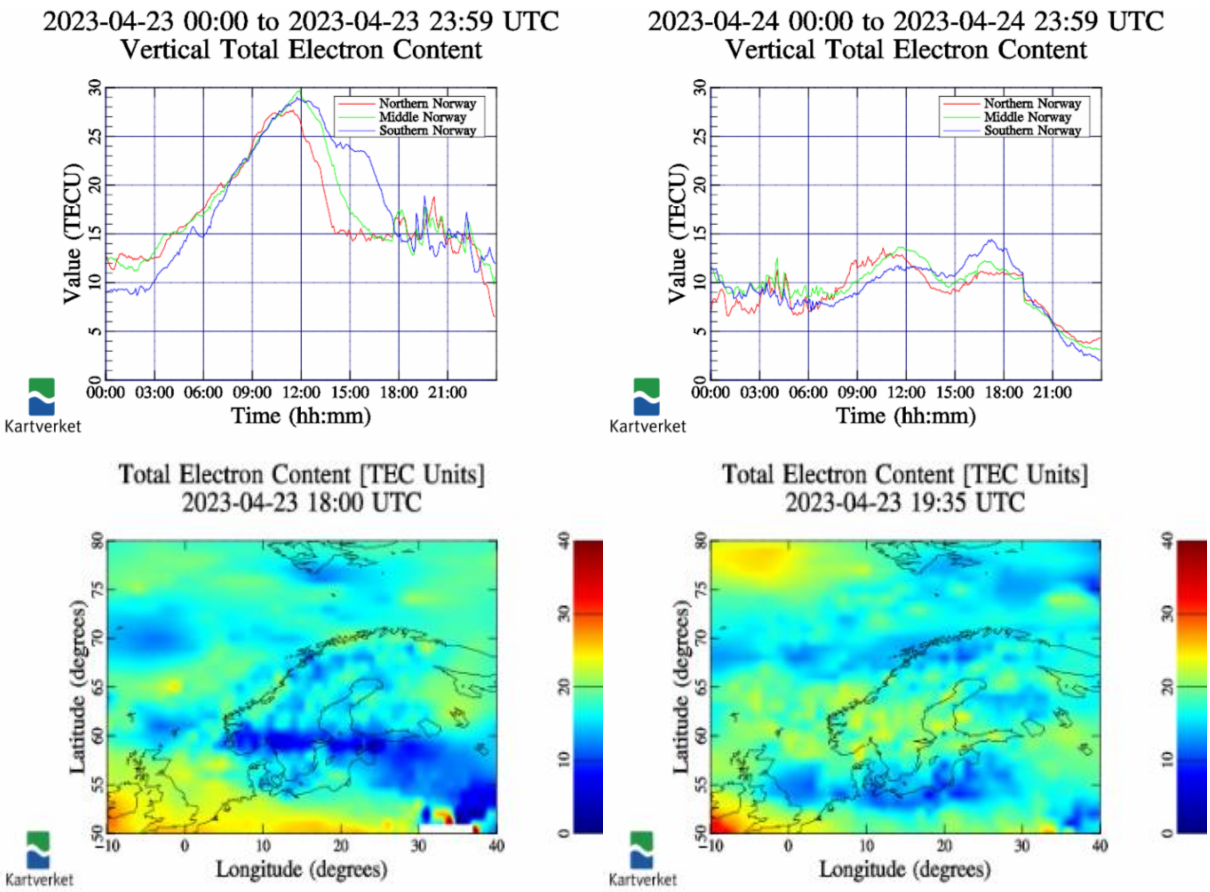

Figure 31*: NMA VTEC conditions (Northern Europe) on 23 April and 24 April. Top: VTEC time series for Norway on 23 April and 24 April. Bottom: VTEC maps for Northern Europe in the evening of 23 April. From product I.107.*

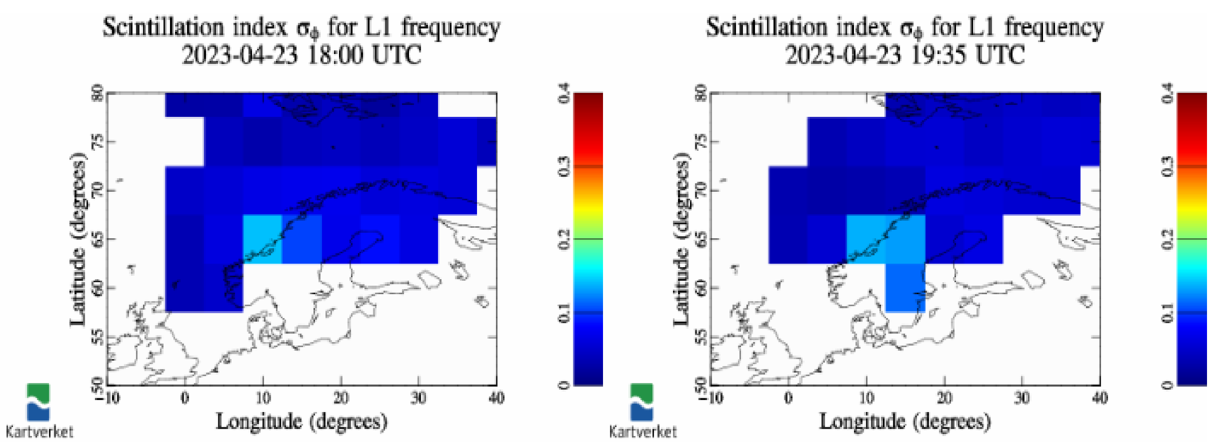

Figure 32*: NMA σφ maps (Northern Europe) in the UTC evening of 23 April. From product I.110b.*

Pre-storm conditions   Storm conditions

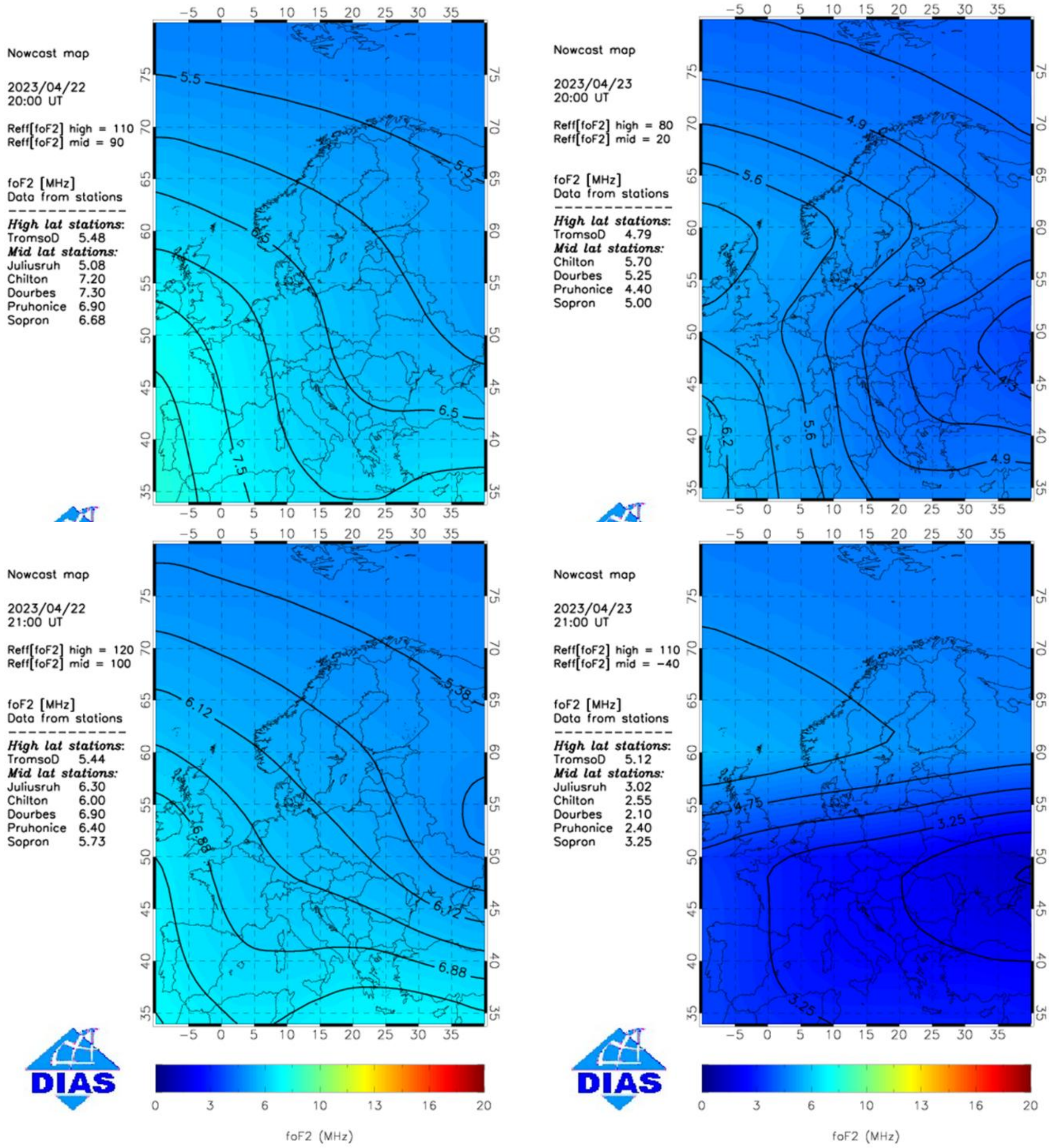

***Figure 33**: NOA/EIS nowcasting foF2 maps for Europe on 22 April (left) and 23 April (right). Maps are based on the SWIF model. From product I.115. Note that the color scale is adjusted to reflect day-night cycle changes. Since Europe was on the night-side during the times reflected in these plots, the values are naturally lower than during the daytime. However, comparing the plots of the 22 April and 23 April at 21:00 UTC one can see a significant reduction of foF2 from ~7MHz to ~3MHz.*

Several alerts were issued by various products part of the network between 23 April at 18:00 UTC and 24 April at 09:00 UTC. An alert for negative storm effects was issued by NOA through the ADA component of the SWIF model at 17:00 UTC on 23 April 2023 and updated at 00:00 UTC on 24 April 2023, based on DISCOVR data at L1 (**Figure 34**, from product I.118, https://swe.ssa.esa.int/dias-federated). A strong depletion in the maximum usable frequency (MUF) from 16:00 UTC on 23 April to 17:00 UTC on 24 April in comparison with quiet conditions on 22 April was also reported. Particularly, disturbed conditions for the MUF for skip-distances of 750 km (MUF750), showing a large decrease, triggered the issue of an alert on 23 April at 20:18:16 UTC (from product I.139):

Message: << ALERT conditions - (Level 3) >>

Date: 2023-04-23
Day Number: 113
Time: 20:18:16 UTC

Disturbed conditions for MUF
-> Large decrease in future MUF

The running estimate of MUF: 6.1 MHz
The 3-hour MUF forecast: 6.4 MHz
The MUF data spread: 1.0 MHz (large)

The 3-hour mean of MUF: 9.5 MHz
The 3-hour standard deviation of MUF: 1.2 MHz

The strong depletion of MUF750 from 23 April at 16:00 UTC to 24 April at 17:00 UTC in comparison with quiet conditions on 22 April is also shown in **Figure 35,** from product I.139, https://swe.ssa.esa.int/impc-federated).

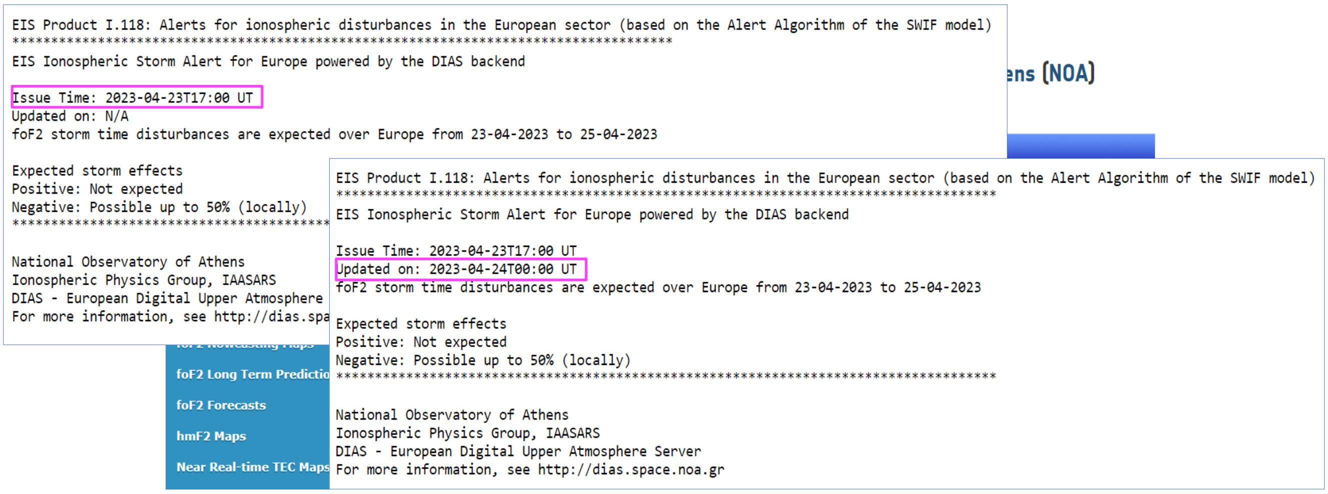

***Figure 34**: EIS ionospheric alerts from product I.118.*

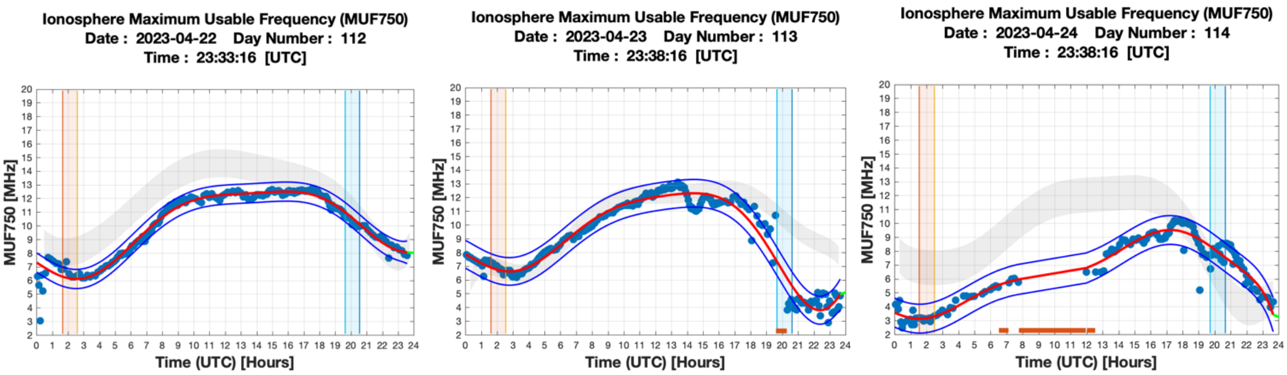

***Figure 35**: DLR/IMPC MUF750 time series on 22 April (left), 23 April (middle), and 24 April (right). From product I.139.*

NOA TechTIDE TEC gradient maps also indicated a strong probability of detection of large scale traveling ionospheric disturbances (LSTIDs). These were triggered by the enhanced auroral activity, as demonstrated by the all-sky image from Kiruna, Sweden on 23 April at 22:11 UTC in **Figure 38** (provided by product G.146, https://swe.ssa.esa.int/irf-aurora-federated). An example of NOA TechTIDE TEC maps comparing quiet conditions at 21:00 UTC on 22 April and storm conditions at 21:00 UTC on 23 April is shown in **Figure 36** (as provided by product I.143, https://swe.ssa.esa.int/web/guest/techtide-federated). TechTIDE LSTID detector maps also demonstrated the occurrence of LSTIDs over Europe with indication about the propagation direction, velocity and amplitude. Two examples of such maps, for 23 April at 19:00 UTC and 21:00 UTC are shown in **Figure 37** (as provided by product I.144).

Quiet conditions Storm conditions

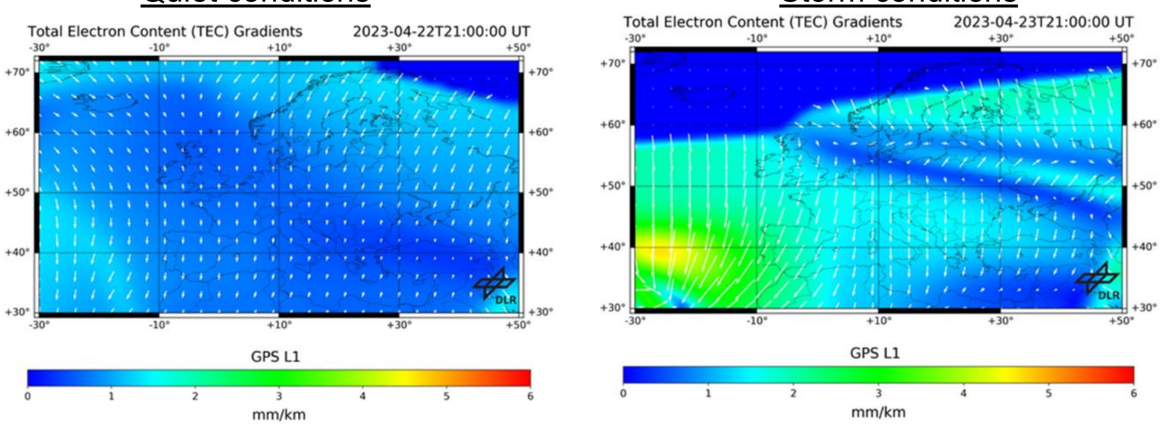

***Figure 36**: TechTIDE TEC gradient maps (Europe) comparing quiet and storm conditions on 22-23 April. From product I.143.*

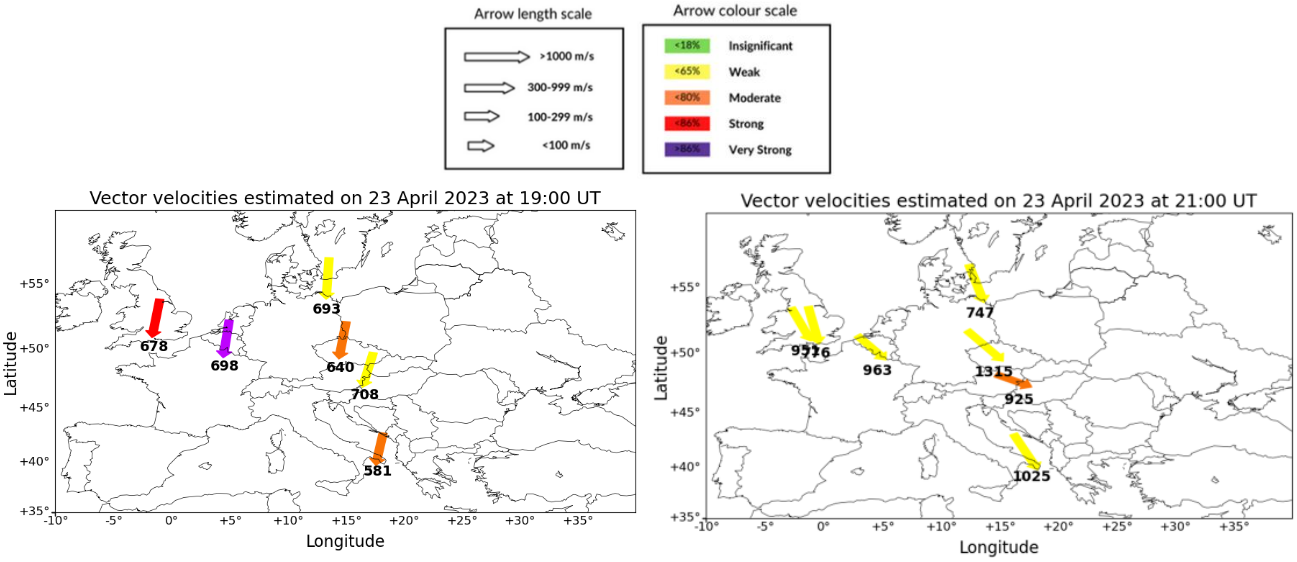

Figure 37. *NOA TechTIDE LSTID detector maps (Europe) at 19:00 UTC and 21:00 UTC on 23 April. The occurrence, propagation direction, velocity and amplitude of LSTIDs is indicated by the colored arrows. From product I.144.*

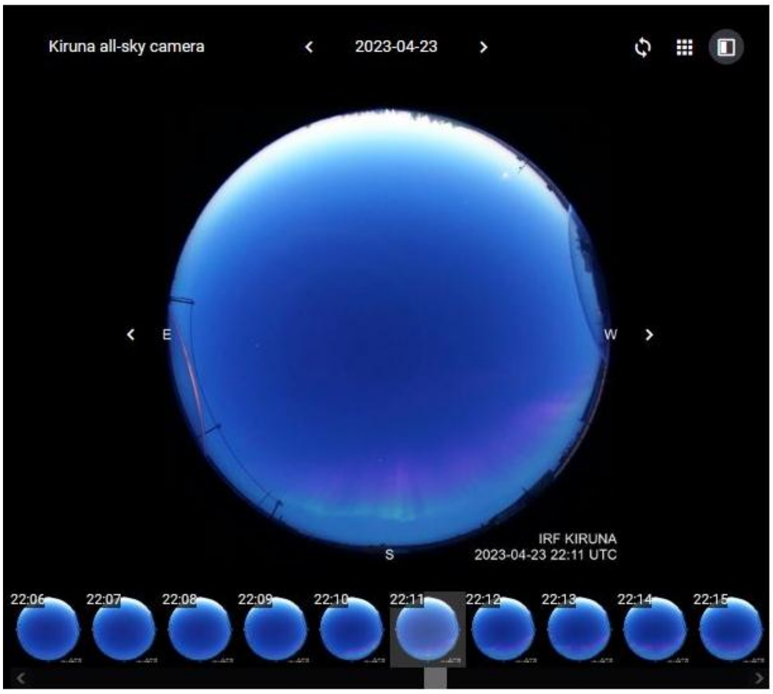

Figure 38: *Auroral data at 22:11 UTC on 23 April from Kiruna, Sweden. From product G.146.*

Impacts on the electron and proton populations at lower altitudes (i.e. radiation belts and slot region) and on the risks for satellite electric charging extended over a longer time window, i.e. through the week following the impact of the interplanetary CME on 23 April. The enhanced electron fluxes at GEO (>0.8-2.0 MeV) due to the arrival of the interplanetary CME on 23 April increased the risk for satellites in orbit to experience dielectric breakdown. Since internal charging is an accumulating process that takes place over periods of the order of several hours to a few days, the risk of dielectric breakdown was present over the course of the following week. **Tables 2, 3** and **4** summarize the nowcast and forecast risks of electrostatic discharge (ESD) at GEO for different materials between 23 April and 30 April. **Table 2** shows that the 24-hour nowcast for Teflon (0.0 mm Al) made on 23 April was liable to experience dielectric breakdown, as provided by product R.178 (https://swe.ssa.esa.int/bira-icea-r178-federated). However, the 24-hour forecast made for 24 April was green (indicating no risk) for all materials for the two scenarios, respectively cables outside (0.0 mm Al) and inside (0.5 mm Al) the spacecraft. The table is green on the 24th because the forecast is based on the electron flux predicted by the NARMAX model, which was lower than the actual GOES electron flux on which the nowcast is based.

	Nowcast	Forecast
Date	**23/04/2023**	**24/04/2023**
Kapton (0.0 mm)		
Polythene (0.0 mm)		
Teflon (0.0 mm)		
Kapton (0.5 mm)		
Polythene (0.5 mm)		
Teflon (0.5 mm)		

Table 2: *Nowcast (middle column) for 23 April 2023 and 24-hour forecast for 24 April 2023 (right column) of ESD risk at GEO for kapton, teflon and polythene. Two shielding scenarios are considered corresponding to cables outside (0.0 mm Al) and inside (0.5 mm Al) the spacecraft (left column). Green means no risk, red is liable to experience dielectric breakdown and grey indicates the result is unavailable. Simulations are performed once a day at 12:00 UTC. From product R.178.*

Table 3 shows the 7-day nowcast for ESD risk at GEO for all materials and scenarios presented in **Table 2**, for the week of 23-29 April. The table shows that the 7-day nowcast for Teflon (0.0 mm Al) continued to be liable to experience dielectric breakdown during the days following 23 April, as provided by product R.179 (https://swe.ssa.esa.int/bira-icea-r179-federated). On 26, 28, and 29 April 2023 the nowcast for Kapton (0.0 mm Al) was also liable to experience dielectric breakdown. On 27 April 2023, no input data was available to run DICTAT (the nowcast was grey). These results are more or less in line with those from the SaRIF products (see **Figure 46**), indicating that the risk for internal charging was higher during the days following 23 April.

Nowcast							
Date	23/04/2023	24/04/2023	25/04/2023	26/04/2023	27/04/2023	28/04/2023	29/04/2023
Kapton (0.0 mm)							
Polythene (0.0 mm)							
Teflon (0.0 mm)							
Kapton (0.5 mm)							
Polythene (0.5 mm)							
Teflon (0.5 mm)							

Table 3*: 7-day nowcast (23-29 April 2023) of ESD risk at GEO for the same materials and shielding scenarios as in* ***Table 2****. Simulations are performed once a day (at 12:00 UTC). From product R.179.*

Table 4 shows the 7-day forecast for ESD risk at GEO for all materials and scenarios presented in **Tables 2** and **3**, for the week of 24-30 April, as provided by product R.180 (https://swe.ssa.esa.int/bira-icea-r180-federated). The table shows that the 24-hour forecast for 24 April 2023 for all materials and for both scenarios made on 23 April 2023 continued to be green during the next days. On 27 April 2023, no input data was available to run DICTAT (24-hour forecast was grey on 28 April 2023).

Forecast							
Date	24/04/2023	25/04/2023	26/04/2023	27/04/2023	28/04/2023	29/04/2023	30/04/2023
Kapton (0.0 mm)							
Polythene (0.0 mm)							
Teflon (0.0 mm)							
Kapton (0.5 mm)							
Polythene (0.5 mm)							
Teflon (0.5 mm)							

Table 4: *7-day forecast (24-30 April 2023) of ESD risk at GEO for the same materials and shielding scenarios as in* ***Tables 2*** *and* ***3****. From product R.180.*

The radiation environment at lower altitudes was also perturbed by the impacting interplanetary CME. **Figure 39** shows the electron flux distributions at 820 km on a geographical map, for the week before the geomagnetic storm (top panel), and for the week following the maximum Kp/minimum Dst were reached in the UTC evening on 23 April (bottom panel). The figures were provided by product R.112 (https://swe.ssa.esa.int/csr-ept-federated). In the bottom panel, the gap (slot) region between the inner belt (South Atlantic Anomaly) and the outer radiation belt (as seen in the top panel) has been filled with electrons during the development of the large geomagnetic storm under discussion. **Figure 40** shows the PROBA-V/EPT high-latitude/polar electron flux survey (from product R.160, https://swe.ssa.esa.int/csr-ept-federated). The electron flux is observed in the outer belt (3<L<5), for three different energies: >0.5 MeV, >1.0 MeV, and >2.0 MeV. An electron flux dropout is observed in the afternoon (UTC) of 23 April (top panel, highlighted in magenta), at storm onset. For comparison, the steady decrease in the Dst index started on 23 April at 11:00 UTC (as shown in **Figure 23**). The electron flux recovered in the night between 23 April (top panel) and 24 April (bottom panel), and was followed by an electron flux enhancement (bottom panel, highlighted in magenta) linked to a Dst increase. The minimum Dst (-212 nT) was reached at 06:00 UTC on 24 April (as shown in **Figure 23**). The geomagnetic storm followed a small SPE that started on 22 April and wherein no protons with E>50 MeV where observed with PROBAV/EPT (marked in yellow in **Figure 41**; from product R.161, https://swe.ssa.esa.int/csr-ept-federated). A small increase (within error bars) in the daily total ionizing dose estimation (behind 2 mm of Al) at LEO due to electrons was observed starting on 24 April (**Figure 42**, top; from product R.167, https://swe.ssa.esa.int/csr-ept-federated). A similar increase was also observed in the daily total non-ionizing dose estimation (**Figure 42**, bottom; from product R.168, https://swe.ssa.esa.int/csr-ept-federated). In both cases, however, the yellow alert color band was not reached.

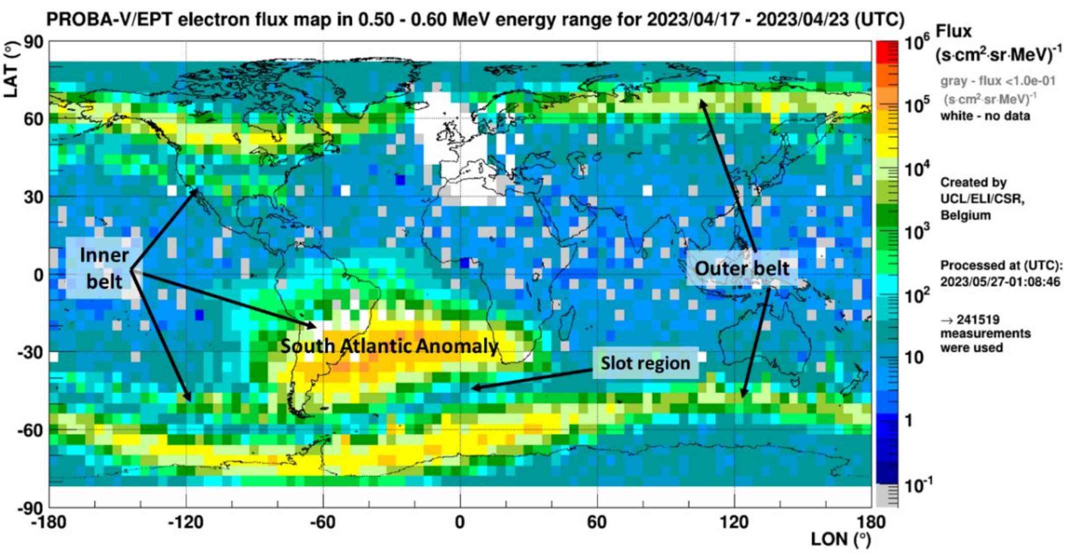

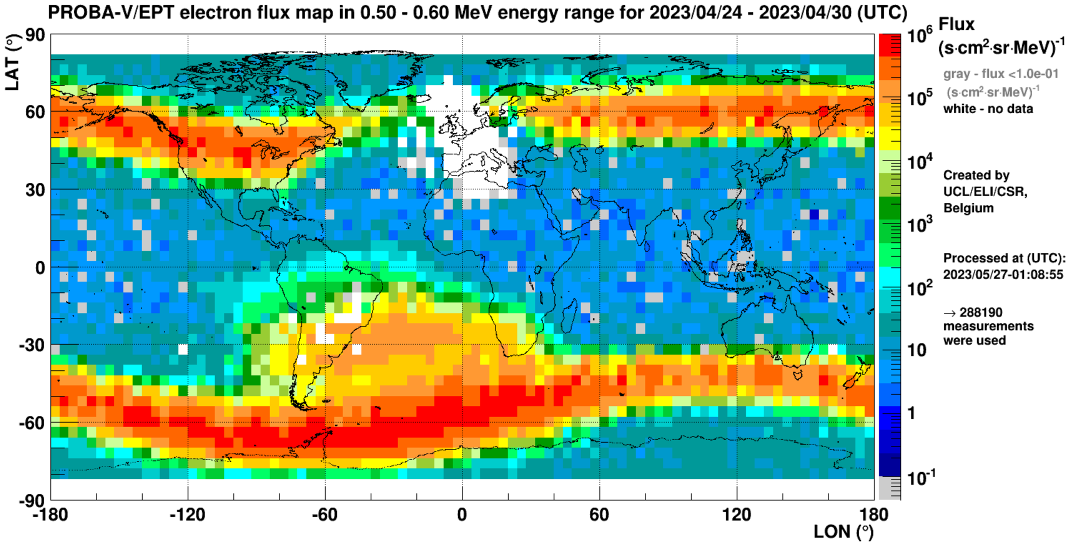

Figure 39*: PROBA-V/EPT global flux maps for electrons in the 0.50-0.60 MeV energy range at 820 km altitude. Top: map for the week before the storm (17-23 April). Bottom: map for the week of the storm (24-30 April). From product R.112.*

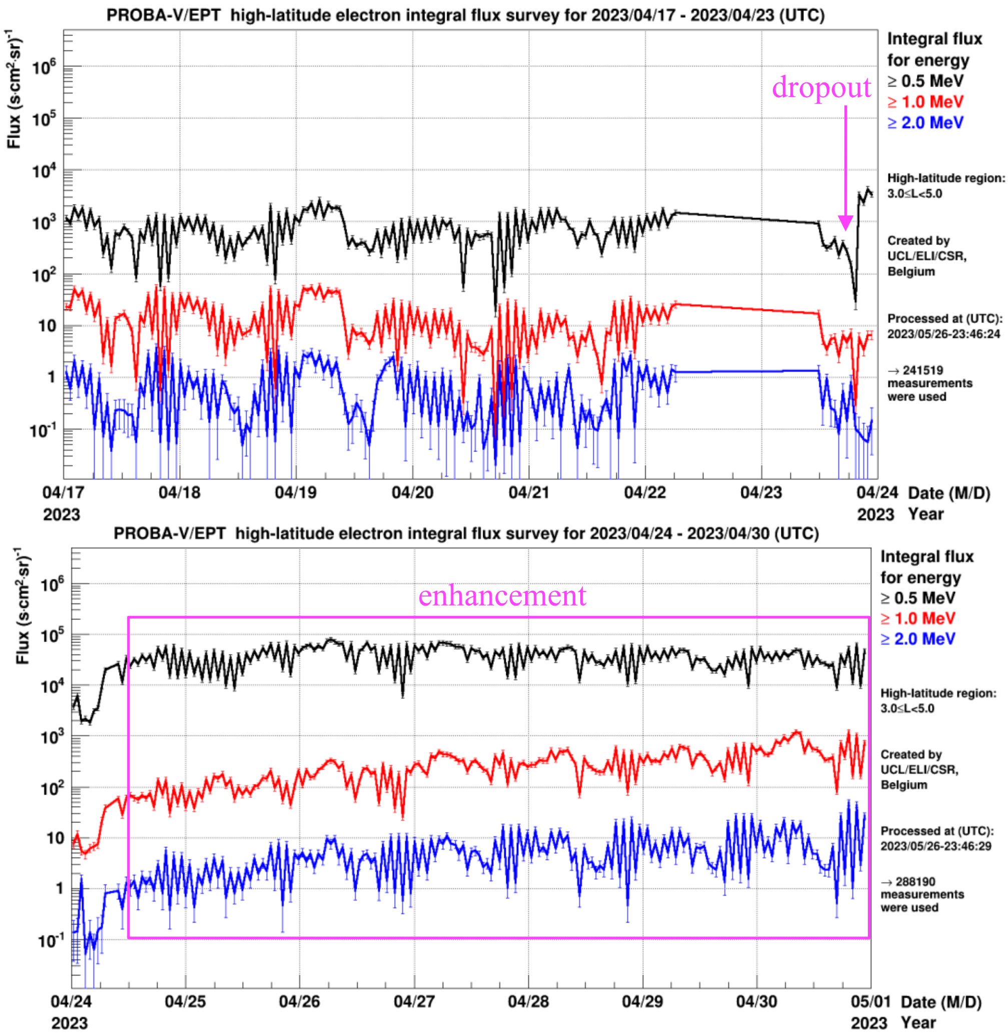

→ THE EUROPEAN SPACE AGENCY

***Figure 40**: PROBA-V/EPT high-latitude electron flux in the outer belt (3<L<5), for three different energies: >0.5 MeV, >1.0 MeV, and >2.0 MeV. Top: map for the week before the storm (17-23 April). Bottom: map for week of the stom (24-30 April). From product R.160.*

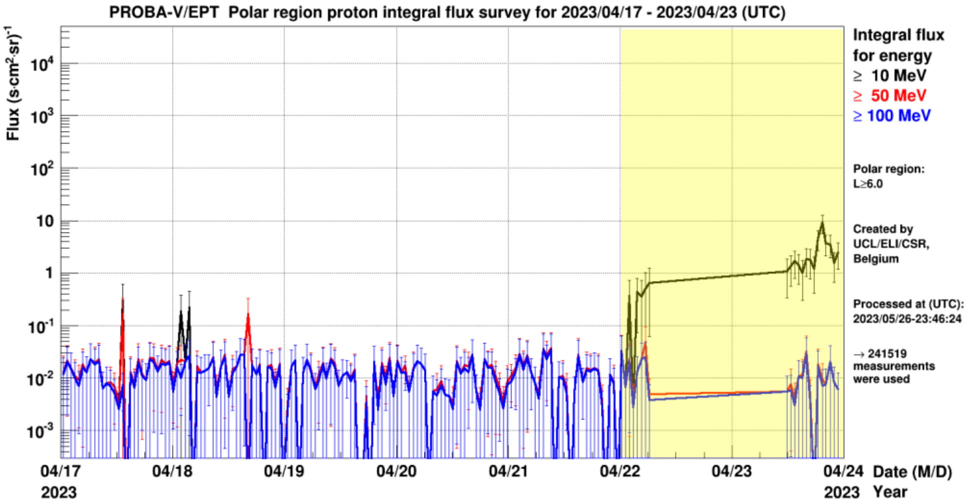

***Figure 41:** PROBA-V/EPT polar proton flux at L>6 for three different energies (>10 MeV, >50 MeV, and >100 MeV), between 17 and 23 April. From product R.161.*

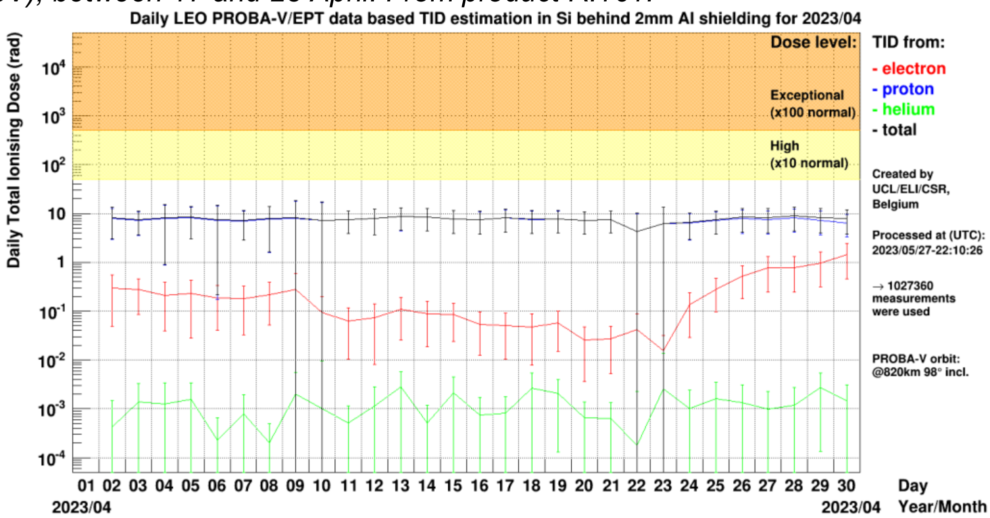

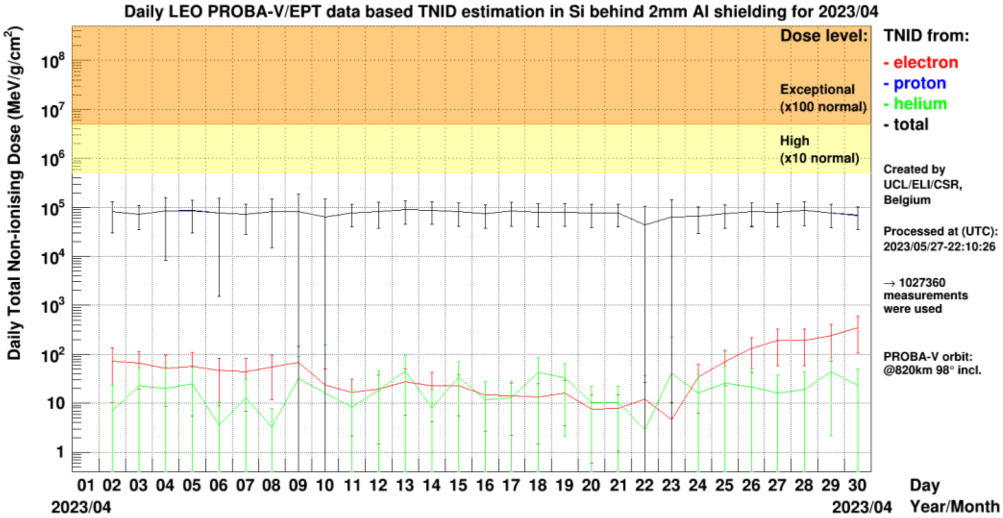

***Figure 42**: PROBA-V/EPT daily total dose estimations (in Si behind 2mm of Al) due to electrons, protons, and helium at LEO, for the month of April 2023. Top: ionizing dose. Bottom: non-ionizing dose. From products R.167 (top) and R.168 (bottom).*

The two radiation belt activity indices Ca4 and Ca8 represent the state of the whole electron radiation belt and characterize, respectively, surface charging and internal charging. The daily data for both indices was available within the network with a one-day delay. There was a moderate risk for surface charging starting on 24 April and ending on 2 May, following the large geomagnetic storm that began on 23 April (as shown in **Figure 43** left, from product R.177: https://swe.ssa.esa.int/onera-rb-ind-federated). The peak of the surface charging risk was met soon after the storm onset, on 24 April. **Figure 43** (right, also from product R.177) shows the tail distribution function of the radiation belt index for surface charging (Ca4) for 24 April 2023. The red line indicates that similar conditions were met during the last one year. A moderate risk for internal charging was also existing, starting on 24 April and ending on 2 May 2023 (**Figure 44** left, from product R.177: https://swe.ssa.esa.int/onera-rb-ind-federated). The peak of the internal charging risk was met 5-6 days after the storm onset, on 29 April. **Figure 44** (right, also from product R.177) shows the tail distribution function of the radiation belt index for internal charging (Ca8) for 24 April 2023. The red line indicates that similar conditions were met during the last one year.

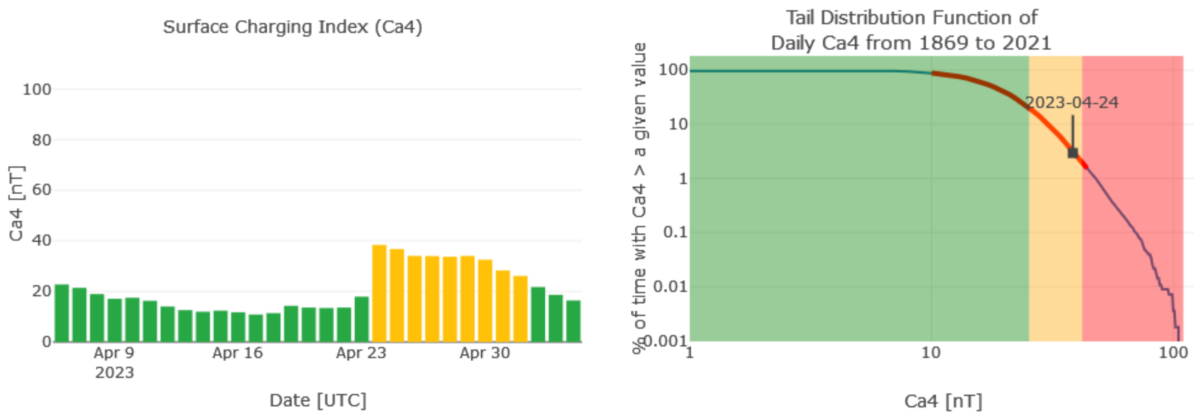

***Figure 43**: RB-IND radiation belt activity index for surface charging (Ca4). Left: Ca4 data for the period of 6 April – 5 May 2023. Right: tail distribution function of daily Ca4 between 1869 and 2021. The red line indicates the span of conditions met in the past one year. From product R.177.*

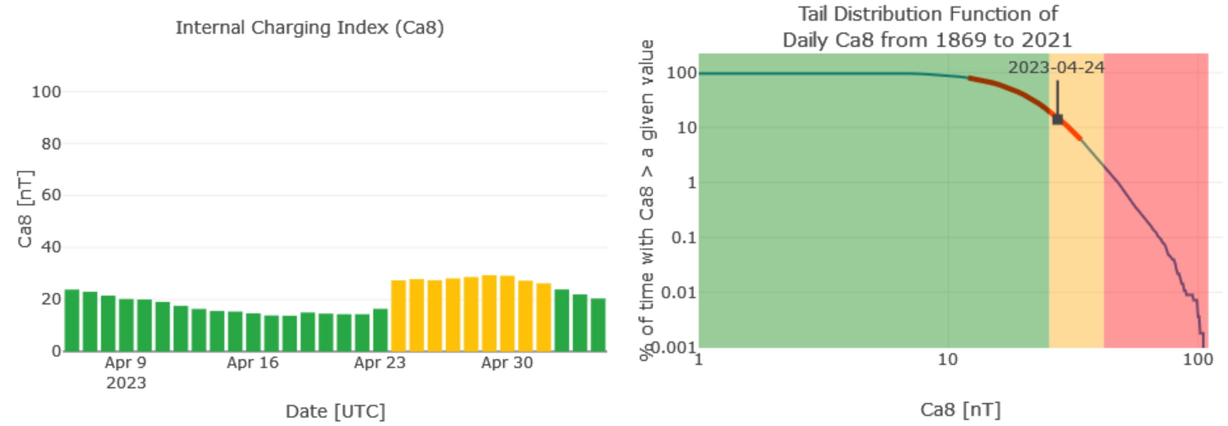

Figure 44: *RB-IND radiation belt activity index for internal charging (Ca8). Left: Ca8 data for the period of 6 April – 5 May 2023. Right: tail distribution function of daily Ca8 between 1869 and 2021. The red line indicates the span of conditions met in the past one year. From product R.177.*

Figure 45 shows the BAS Radiation Belt Model (BAS-RBM) relativistic electron forecast issued on 28 April and covering the period 21-28 April (observations) and 28-29 April (forecast), as part of the SaRIF Radiation Environment Products (https://swe.ssa.esa.int/sarif-federated). **Figure 45** (top left) shows the electron flux (colour coded) as a function of L* and time, at >2.0 MeV and pitch angle of 88 degrees from BAS-RBM. On 22 April, the flux was fairly constant at a relatively low level (10 to 100 cm^{-2} s^{-1} sr^{-1}). In the UTC afternoon of 23 April, when the storm started, there was a sharp increase in the solar wind velocity and pressure, compressing the magnetopause and causing the last closed drift shell (LCDS, shown as a white line) to move inside geostationary orbit (the dashed black line), resulting in a rapid depletion of the electron flux. This was followed by another incursion that came close to GEO and further depleted the flux, mainly by rapid outward transport. After this, the flux started to recover and gradually increased over the next few days, significantly exceeding its pre-storm level by 26 April. **Figure 45** (bottom left) shows the electron flux at the location of the satellite from the model (in red), together with satellite observations from GOES-16 when they are available (in black). These measurements are around the noise level of the instrument and so cannot show the significant drops in flux associated with the movement of the magnetopause inside GEO. **Figure 45** (top right) shows the electron flux (colour coded) as a function of L*[1] and time, at >2.0 MeV and 2.0 MeV and pitch angle of 88 degrees taken from the BAS-RBM. A significant injection of electrons into the slot region (at L*=2.2, approximately at 8000 km of altitude) occurs on the 23 April 2023 during the peak activity of the storm. The flux in the slot region then decays slowly over

[1] The distinction between L and L* is explained in Roederer, J. G., & Lejosne, S. (2018).

the next few days. **Figure 45** (bottom right) panel shows the electron flux. No data is shown on this plot as the Van Allen Probes data is no longer available. When the storm occurs on 23 April, the flux increases rapidly by several orders of magnitude from its pre-storm level, as enhanced radial transport moves flux into the slot region from the outer belt. The flux then decays slowly over the next few days but is still significantly enhanced on 29 April.

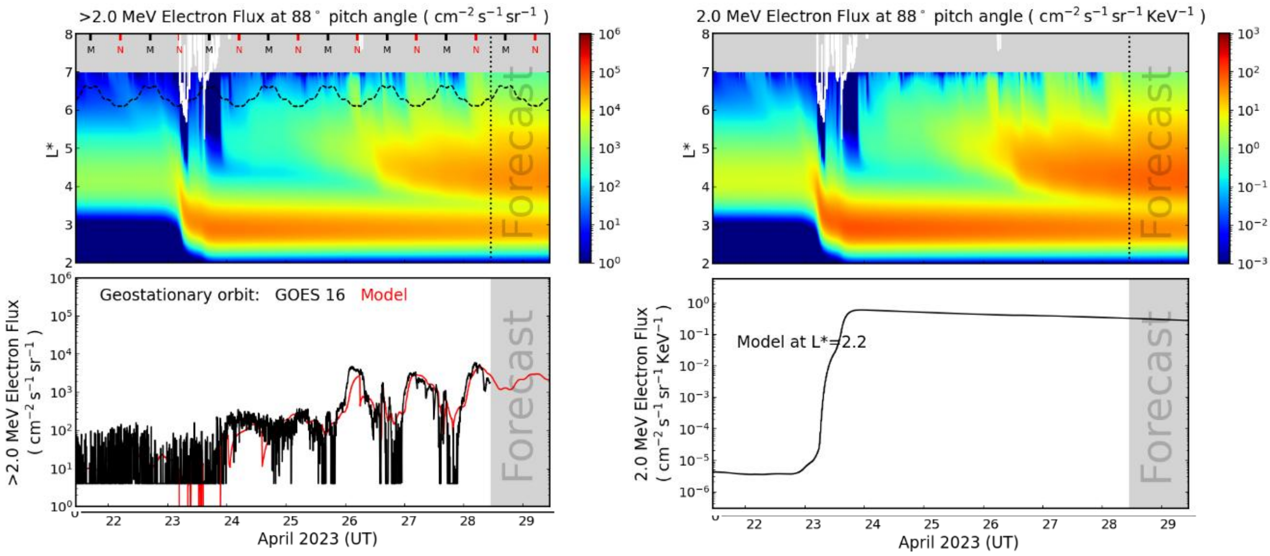

Figure 45:** BAS-RBM relativistic electron forecast issued on 28 April and covering the period 21-28 April (observations) and 28-29 April (forecast).** *Top left: electron flux at >2.0 MeV and pitch angle of 88 degrees taken from the BAS-RBM, as a function of L* and time. GOES-16 measurements are indicated by the dashed black line. Bottom left: integrated >2.0 MeV electron flux as a function of time, from GOES-16 (in black) and from BAS-RBM (in red). Top right: electron flux at 2.0 MeV and pitch angle of 88 degrees taken from the BAS-RBM, as a function of L* and time. Bottom right: integrated 2.0 MeV electron flux as a function of time in the slot region (L*=2.2), from BAS-RBM. From products R.145 and R.154.*

The SaRIF Internal Satellite Charging Products (https://swe.ssa.esa.int/sarif-federated) also highlighted a risk of internal satellite charging due to high energy electrons in GEO, MEO, and the slot region starting from 24 April 2023 and following the high-speed solar wind conditions and large geomagnetic storm that began on 23 April 2023. **Figure 46** shows that the risk for internal charging occurring in GEO reached Level 3 on 24 April 2023, increased to Level 4 on 26 April around 12:00 UTC, went back to Level 3 late in the evening, but returned to level 4 at times on 27 and 28 April as the flux at GEO increased. The large dips in the charging current on 23 and 24 April occur when the spacecraft is outside the LCDS and shortly afterwards when the flux is still being depleted by outward radial transport. **Figure 47** shows that the risk for internal charging occurring in MEO reached Level 4 on the 23 April, dropped to Level 3 on 24 April, increased to Level 4 late on 25 April where it remained for the following days. **Figure 48** shows that the risk for internal charging occurring in the slot region reached Level 3 on 24 April and returned to Level 2 late on 25 April where it remained on 26-28 April.

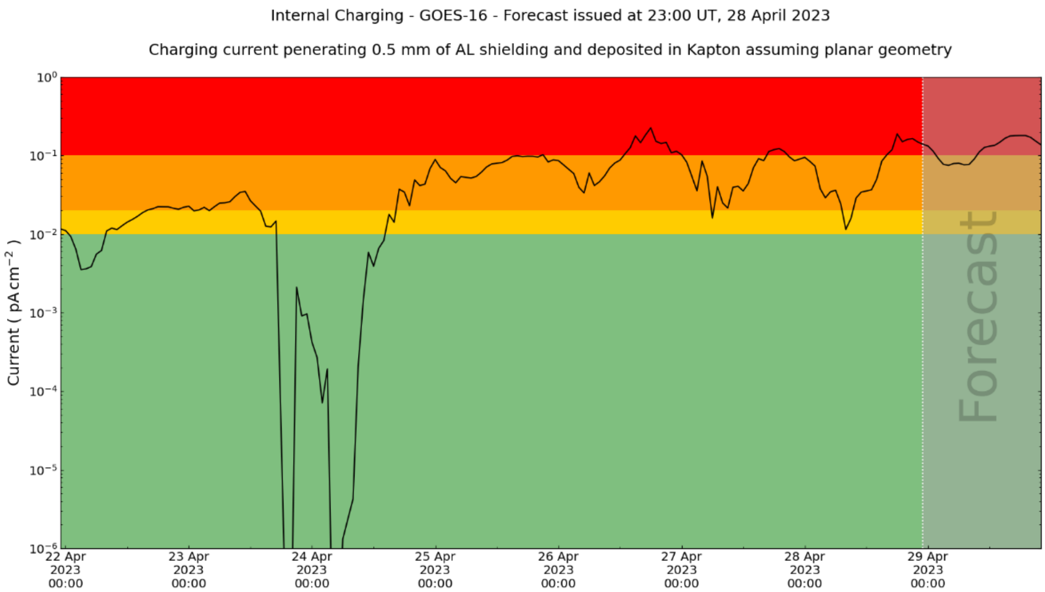

***Figure 46**: Risk of internal satellite charging due to high energy electrons in GEO issued on April 28 and covering the period 22-28 April (observations) and 29 April (forecast). From product R.143.*

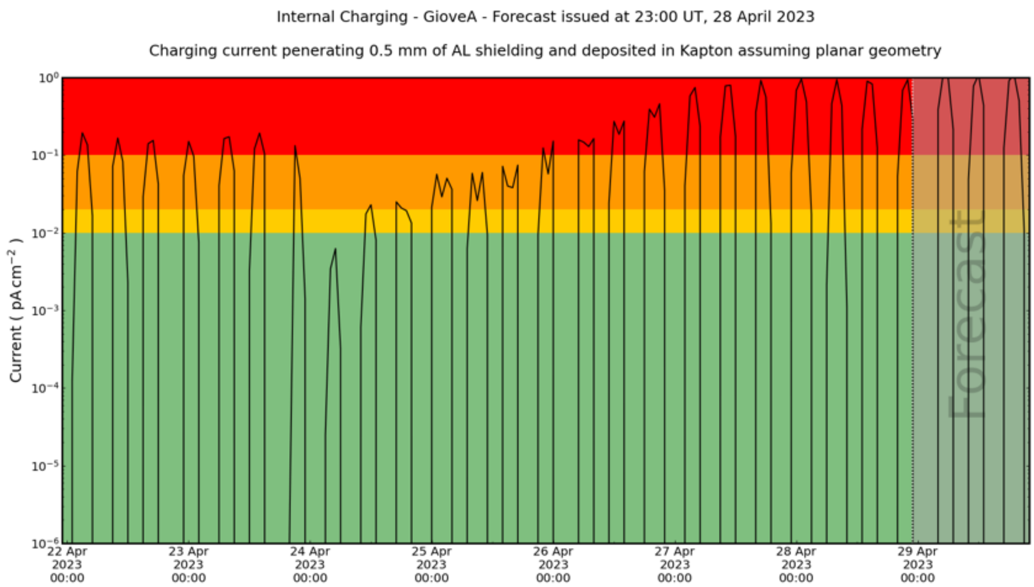

***Figure 47**: Risk of internal satellite charging due to high energy electrons in MEO issued on 28 April and covering the period 22-28 April (observations) and 29 April (forecast). From product R.149.*

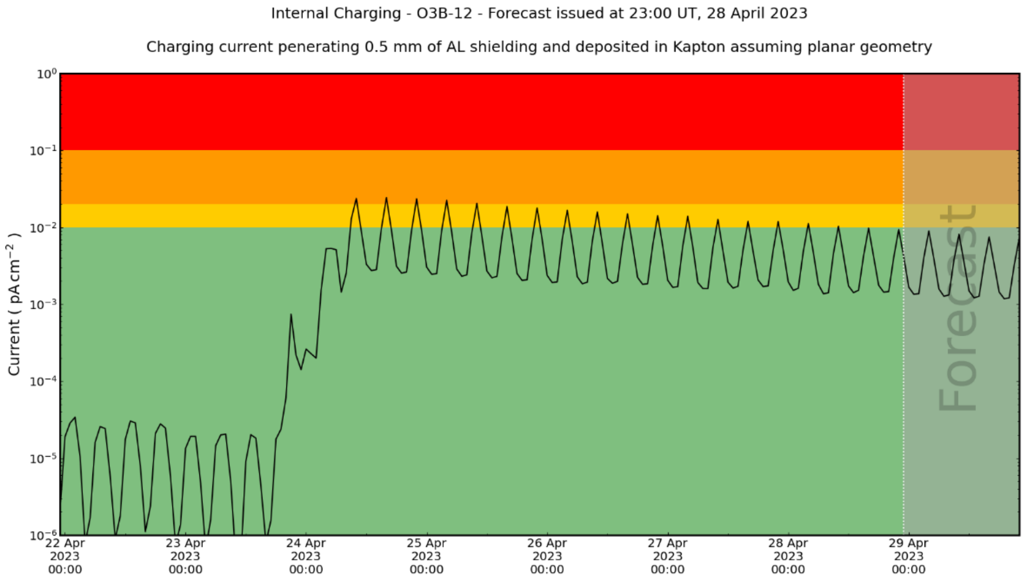

***Figure 48**: Risk of internal satellite charging due to high energy electrons in the slot region, issued on April 28 and covering the period April 22-28 (observations) and April 29 (forecast). From product R.152.*

MOSWOC relativistic electron forecasts from the Relativistic Electron Forecast Model (REFM) at GEO, part of the SaRIF product suites (https://swe.ssa.esa.int/sarif-federated), were also issued during and after the storm. On 25 April, the associated 24-hour integrated fluence was predicted to show a rising trend through 25-26 April, with a chance of reaching Active conditions (corresponding to 1e8 integrated pfu or higher), followed by a decline on 27-28 April (**Figure 49**, top[2]). However, the observed trend (measured and forecast) only reached its maximum on 28 April, when it indeed reached Active conditions. A decreasing trend then followed through 3 May (**Figure 49**, bottom). Overall, the 24-hour integrated fluence closely followed the high-speed solar wind conditions (shown in **Figure 14**) and large geomagnetic storm that began on 23 April (shown in terms of the Kp and Dst indices in Figures **22** and **23**).

[2] The probability table on the right-hand side of the figure (top and bottom) provides probabilistic forecasts for >2 MeV high energy electron fluence at GEO, over the next 4-days. It shows the probability of exceedance of the Active ($1x10^8$ cm^{-2} sr^{-1} day^{-1}) and Very Active ($1x10^9$ cm^{-2} sr^{-1} day^{-1}) thresholds.

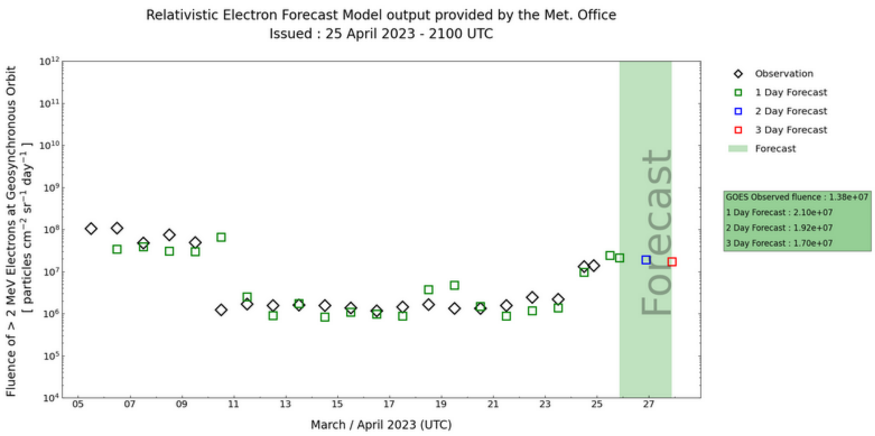

High Energy Electron Event Forecast

Issued 2023-04-25T00:08:53

Probability of threshold exceedance

	Active	V.Active
Day 1	30%	1%
Day 2	50%	1%
Day 3	30%	1%
Day 4	20%	1%

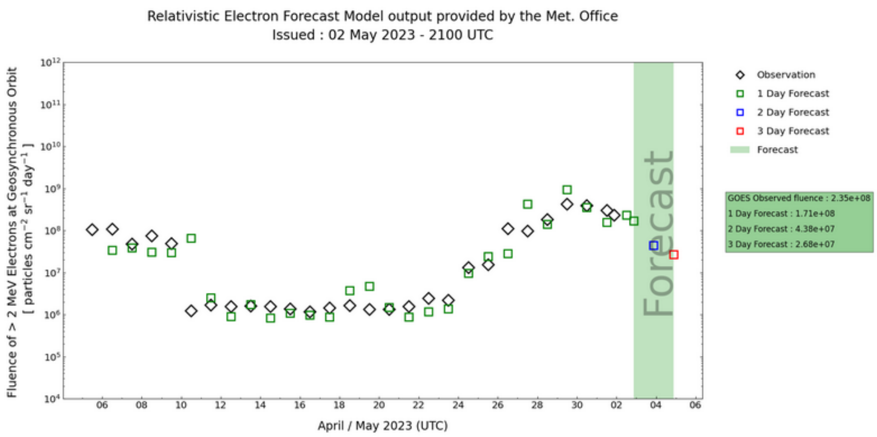

High Energy Electron Event Forecast

Issued 2023-05-02T00:11:00

Probability of threshold exceedance

	Active	V.Active
Day 1	100%	5%
Day 2	70%	5%
Day 3	60%	1%
Day 4	50%	1%

***Figure 49**: MOSWOC relativistic electron forecast at GEO from the REFM model. Top: forecast issued on 25 April. Bottom: forecast issued on 2 May. The green tables (right side of the plots) show the latest observed fluences at GOES, and the most recent fluence predictions for the next 1-3 days. From product R.155.*

Figure 50 shows the forecast for the plasmasphere electron density from the SWIFF Plasmasphere (SPM) electron density model for 23 April (top), 24 April (middle), and 25 April (bottom) (from product R.136, https://swe.ssa.esa.int/bira-swiff-federated). At the beginning of 23 April, the Kp index was still quite low (Kp=4, as shown in **Figure 22**), so that the plasmasphere was quite extended and almost circular in the equatorial plane. As the planetary geomagnetic activity index Kp began to increase, the plasmasphere started eroded. The planetary geomagnetic activity increased and reached its maximum value of Kp=8 between the evening of 23 April and the morning of 24 April, before to slowly start to decrease. On 24 April, the plasmasphere was highly eroded and a plasmaspheric plume appeared in the dusk sector due to the increase of geomagnetic activity. On 25 April, the plasmasphere slowly returned to its normal quiet state as the planetary geomagnetic activity index Kp continued to decrease. The Kp was still high and increasing at 00:00 UTC, which led to a plasmapause very dependent on the Magnetic Local Time (MLT).

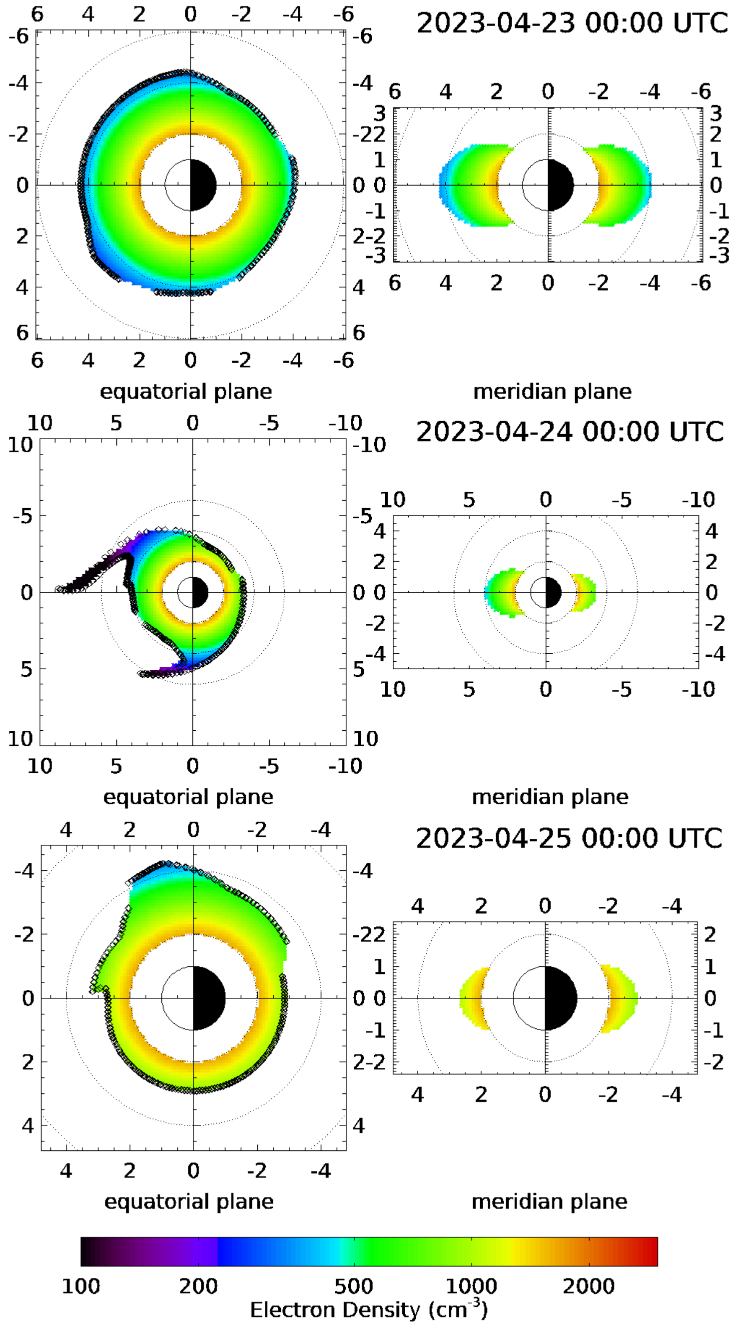

***Figure 50**: forecast for the plasmasphere electron density for 23 April (top), 24 April (middle), and 25 April (bottom), based on the SPM model. From product R.136.*

The SREM daily situation reports (products R.118 and R.119, https://swe.ssa.esa.int/pb-srem-federated) aim to provide a concise overview of the proton and electron radiation levels in key-regions of space on a daily basis.

On 23 and 24 April (not shown), the proton inner belt radiation level remained close to its long-term average level. The electron inner belt and electron slot region were at a very low level, and the electron outer belt radiation level was low. The proton inner belt and electron inner belt radiation levels remained nearly unchanged during the following weeks. On 25 April, a sudden increase in the electron slot region radiation level was observed by PROBA-1 (**Figure 51**, top). The level further increased and reached its maximum on 27 April (**Figure 51,** middle). At its maximum, the level was approximately a factor 140 higher than predicted by the AP8/AE8 maximum model, and a factor 500 higher than predicted by AP8/AE8 minimum model. From 28 April (**Figure 51**, bottom) onwards, the electron slot region radiation level slowly decreased. It is, however, only by the end of May 2023 that it reached pre-event level again.

In contrast to the slot region, the electron radiation level in the electron belt showed little changes on 25 April. It only started to show enhanced levels on 26 April. The level continued to increase in the following days to reach a maximum on 1 May. It remained at high levels until 6 May when it dropped below AE8 model predictions. The electron radiation level in the electron belt region is normally quite volatile and changes of the level of several orders of magnitude within a few days are regularly observed. Such changes are often associated with high-speed solar wind and southward IMF Bz component. Strong changes of the electron radiation level as observed after 25 April in the slot region are, however, much rarer. Normally, changes of the high energy electron flux in the electron belt do not significantly propagate to lower L values. The radiation level in the slot region is hence much more stable than the level in the electron belt. In this case, however, it seems that electrons were 'pushed' into the slot region by the violent event on 24-25 April, which caused the sudden increase of the observed level on 25 April. After that, however, the new particle population in the slot region seemed to be unaffected by the ongoing variations of the radiation levels in the electron belt and slowly decayed over the following weeks. On 28 April, INTEGRAL was in this region and saw an increase in the electron outer belt radiation level. This is consistent with what was observed by PROBA-1 in the electron outer belt on the same day (**Figure 51**, bottom).

2023-04-24 | 20230425 | 2023-04-26

space region	#1	#2	#3	#4	#5	#6	#7	#8
	Proton belt	Proton belt	Slot region	Electron belt	Electron belt	Interplanetary	Interplanetary	Interplanetary
particle	protons	electrons	electrons	electrons	electrons	cosmics/protons	cosmics/protons	cosmics/protons
satellite	PROBA1	PROBA1	PROBA1	PROBA1	Integral	Integral	Herschel/Planck	Rosetta
L-range	1.2 ≤ L ≤ 1.3	1.6 ≤ L ≤ 1.7	2.5 ≤ L ≤ 3.0	4.0 ≤ L ≤ 5.0	6.0 ≤ L ≤ 7.0	see orbit	L2	no orbit available
status	on-going	on-going	on-going	on-going	on-going	on-going	mission completed	mission completed
radiation levels relative to								
AE8/AP8 min	0.5	0.0	128.5	0.3	-			
AE8/AP8 max	0.7	0.0	35.1	0.2	-			
SREM average	1.0	0.0	6.5	0.1	-	0.8	-	-
SEP alarm						no SEP	-	-

2023-04-26 | 20230427 | 2023-04-28

space region	#1	#2	#3	#4	#5	#6	#7	#8
	Proton belt	Proton belt	Slot region	Electron belt	Electron belt	Interplanetary	Interplanetary	Interplanetary
particle	protons	electrons	electrons	electrons	electrons	cosmics/protons	cosmics/protons	cosmics/protons
satellite	PROBA1	PROBA1	PROBA1	PROBA1	Integral	Integral	Herschel/Planck	Rosetta
L-range	1.2 ≤ L ≤ 1.3	1.6 ≤ L ≤ 1.7	2.5 ≤ L ≤ 3.0	4.0 ≤ L ≤ 5.0	6.0 ≤ L ≤ 7.0	see orbit	L2	no orbit available
status	on-going	on-going	on-going	on-going	on-going	on-going	mission completed	mission completed
radiation levels relative to								
AE8/AP8 min	-	0.0	532.2	4.3	-			
AE8/AP8 max	-	0.0	145.4	2.8	-			
SREM average	-	0.0	31.3	1.2	-	0.8	-	-
SEP alarm						no SEP	-	-

2023-04-27 | 20230428 | 2023-04-29

space region	#1	#2	#3	#4	#5	#6	#7	#8
	Proton belt	Proton belt	Slot region	Electron belt	Electron belt	Interplanetary	Interplanetary	Interplanetary
particle	protons	electrons	electrons	electrons	electrons	cosmics/protons	cosmics/protons	cosmics/protons
satellite	PROBA1	PROBA1	PROBA1	PROBA1	Integral	Integral	Herschel/Planck	Rosetta
L-range	1.2 ≤ L ≤ 1.3	1.6 ≤ L ≤ 1.7	2.5 ≤ L ≤ 3.0	4.0 ≤ L ≤ 5.0	6.0 ≤ L ≤ 7.0	see orbit	L2	no orbit available
status	on-going	on-going	on-going	on-going	on-going	on-going	mission completed	mission completed
radiation levels relative to								
AE8/AP8 min	0.3	0.0	211.4	5.6	2.3			
AE8/AP8 max	0.5	0.0	57.6	3.7	2.3			
SREM average	1.0	0.1	10.9	1.5	2.3	0.8	-	-
SEP alarm						no SEP	-	-

***Figure 51**. Time series of PROBA-1/SREM radiation rates from the SREM space radiation situation reports (product R.118) on 25 April (top), 27 April (middle), and 28 April (bottom). Of relevance for this report are (highlighted in magenta): the PROBA-1 values for the proton inner belt (#1), the electrons in the inner proton belt region (#2), electron slot region (#3), and electron outer belt (#4); and the INTEGRAL electron outer belt radiation level (#5).*

Finally, the network also captured the impacts of this event on ground-based systems. **Figure 52** shows the Geomagnetic Induced Current (GIC) along the Finnish natural gas pipeline as 1-min values at Mäntsälä in southern Finland from 23 April 2023 at 12 UTC, to 24 April 2023 at 12 UTC (snapshot from archived plots from FMI products, https://swe.ssa.esa.int/fmi-federated). Note that there is some noise in the measured GIC. The largest measured GIC value in relation to this event, based on 10-s data, was about 35 A in the morning (UTC) of 24 April. This GIC event ranks in the top 5 daily maxima since the recordings started in November 1998. The record-high value is 57 A (29 October 2003).

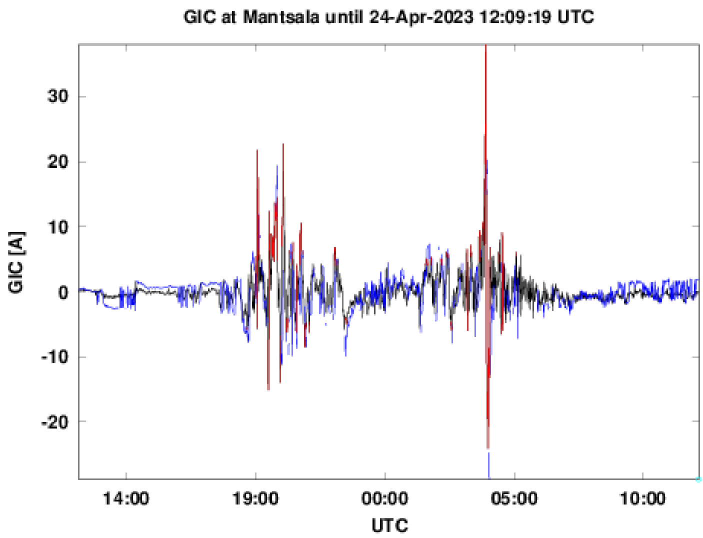

Figure 52. *Modelled (black) and measured (blue) GICs at pipeline in Mäntsälä. The blue line is the measured value (positive eastward) and black is the modelled value. Red values mark modelled GICs exceeding the top 0.1% of all values in long-term statistics in 1996-2008. From product G.114 https://swe.ssa.esa.int/fmi-federated.*

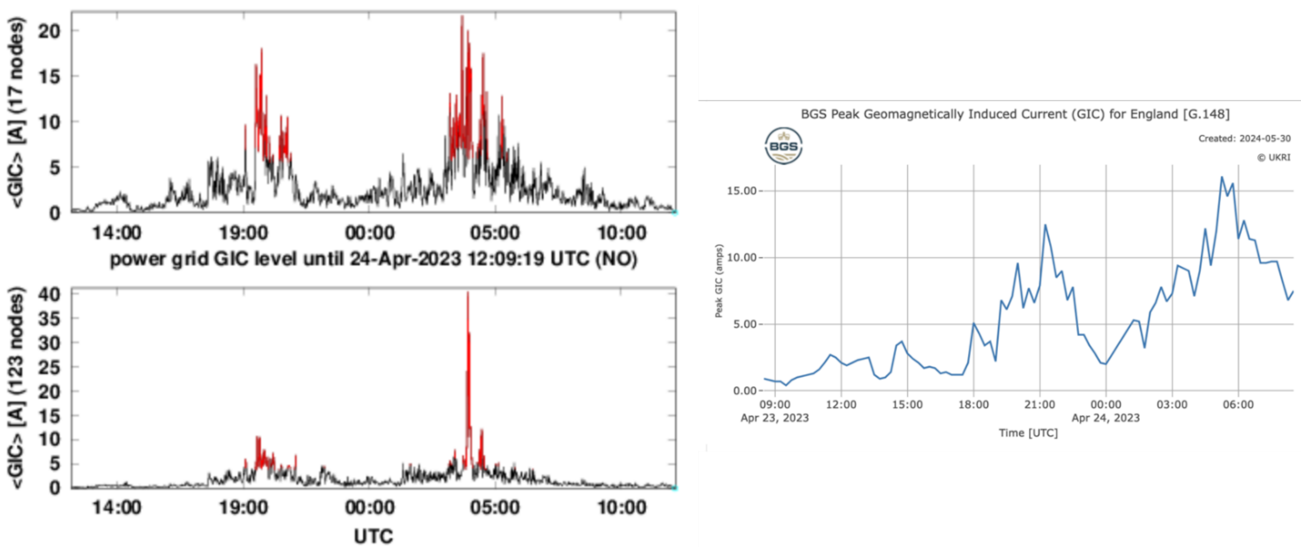

Figure 53. *Modelled GICs for high-voltage power grids in Finland (top) and Norway (bottom) from product G.111. Red values mark modelled GICs exceeding the top 0.1% of all values in long-term statistics in 1996-2008. From https://swe.ssa.esa.int/fmi-federated. G.148 Peak Geomagnetically Induced Current (GIC) for England to the right from https://swe.ssa.esa.int/BGS-federated.*

Figure 53 shows the modelled average GIC as 1-min values at the substations of the Finnish (FI, top left) and Norwegian (NO, bottom left) high-voltage power grids from 23 April 2023 at

12 UTC to 24 April 2023 at 12 UTC (snapshots from archived plots from product https://swe.ssa.esa.int/fmi-federated**).** Several periods indicate the modelled GICs exceeded the top 0.1% of all values in long-term statistics in 1996-2008 (shown in red). Comparison to the pipeline GIC plot (**Figure 52**) shows simultaneous high activity as expected. In Norway (**Figure 53**, bottom left), there is relatively larger GIC activity around 24 April at 04:00 UTC than in Finland (**Figure 53**, top left). Note that the grid models used here are simplified and do not correspond to the true configurations. The peak GIC in England from April 23-24 is shown in the Figure 17 to the right. The largest absolute value (in Amps) modelled for any substation in the power network within England, here seen values over 15 Amps on April 24.

From April 25 the perturbations in the solar wind and resultant geomagnetic activity were in decline indicating the end of the main event. However, as mentioned the impact of the event could still be seen for a number of days after this time in some data products, for example in the delayed impact on the electron flux, relevant for spacecraft charging.
This report has highlighted how this interesting and rare event was captured by the ESA SWE network and much of which can still be explored by the user in the archive feature of many products.

4 TECHNICAL DETAILS

4.1 Products Considered

The products used in this report are listed below. For more technical information about individual products, see the product catalogue [RD-PROD] and help pages of individual products.

S-ESC:

- INAF/OACT sunspot characteristics (S.123a): https://swe.ssa.esa.int/catania-S123a-federated
- INAF/OACT Halpha Solar Images (S.122): https://swe.ssa.esa.int/catania-S122-federated
- SIDC EUV flare detection (S.127): https://swe.ssa.esa.int/sidc-S127-federated

- SIDC Solar flare forecast (S.109b): https://swe.ssa.esa.int/sidc-S109b-federated
- SIDC Solarmap (S.101c): https://swe.ssa.esa.int/web/guest/sidc-S101c-federated
- SIDC SDO/AIA images (S.106): https://swe.ssa.esa.int/sidc-S106-federated
- SIDC CACTus CME detection (S.111): https://swe.ssa.esa.int/sidc-S111-federated
- SIDC CACTus Halo CME alert (S.112b): https://swe.ssa.esa.int/sidc-S112b-federated
- SIDC Daily space weather bulletin (S.110): https://swe.ssa.esa.int/sidc-S110-federated
- UNIGRAZ/KSO filament detection (S.107f): https://swe.ssa.esa.int/kso-S107f-federated
- ASUCAS/SPS solar flare forecast (S.501a): https://swe.ssa.esa.int/sps-S501a-federated
- ASUCAS/SPS sunspot group characteristics (S.123d): https://swe.ssa.esa.int/sps-S123d-federated
- UPSaclay/MEDOC Maps of electric currents in active regions (S.052a): https://swe.ssa.esa.int/medoc-S052a-federated

H-ESC:

- STFC/RAL Space H-ESC archive product browser (H.113a): https://swe.ssa.esa.int/ral-hparc-pb-federated
- UKMO Near-Earth solar wind forecasts (Enlil Ensemble) (H.101a): https://swe.ssa.esa.int/metoffice-enlil-e-federated
- UKMO Near-Earth space weather notifications product (H.106a): https://swe.ssa.esa.int/metoffice-alerts-e-federated
- STFC/RAL Space Near-Earth solar wind forecasts (EUHFORIA) (H.101g): https://swe.ssa.esa.int/ral-euhforia-e-federated
- STFC/RAL Space Solar Wind Forecast Speed Comparison (H.101z): https://swe.ssa.esa.int/ral-swfsc-e-federated
- STFC/RAL Space H-ESC product assessment Report (H.112a): https://swe.ssa.esa.int/ral-hparc-par-federated
- STFC/RAL Space STEREO-A HI Time Elongation Annotated J-Maps (Beacon Mode) (H.120c) https://swe.ssa.esa.int/ral-stahi-h120c-federated
- DTU Space Automated WARnings of Earth arrivals (AWARE) (H.106b): https://swe.ssa.esa.int/dtu-aware-federated

- DTU Space Automated WARnings of STEREO_A arrivals (AWARE_A) (H.110b): https://swe.ssa.esa.int/dtu-aware-a-federated
- UNIGRAZ/IGAM CME arrival time predictions (Drag Based Ensemble Model Tool) (H.108b): https://swe.ssa.esa.int/graz-dbem-federated
- KU Leuven/Virtual Space Weather Modelling Centre (VSWMC) (H.200a): https://swe.ssa.esa.int/kul-cmpa-federated
- INAF Magnetic Effectiveness Tool (MagEffTool) (H.103d): https://swe.ssa.esa.int/inaf-mageff-federated

R-ESC:

- SPARC EDRS-C/NGRM L2 Electron differential fluxes (R.170): https://swe.ssa.esa.int/sparc-geo-ngrm-r170-federated
- SPARC EDRS-C/NGRM L2 Proton differential fluxes (R.171): https://swe.ssa.esa.int/sparc-geo-ngrm-r171-federated
- NOA/IAASARS HESPERIA REleASE (R.158): https://swe.ssa.esa.int/noa-hesperia-federated
- ICEA Internal charging environment and analysis report (R.178): https://swe.ssa.esa.int/bira-icea-r178-federated
- ICEA Internal charging environment nowcast (R.179): https://swe.ssa.esa.int/bira-icea-r179-federated
- ICEA Internal charging environment forecast (R.180): https://swe.ssa.esa.int/bira-icea-r180-federated
- PROBA-V/EPT: https://swe.ssa.esa.int/csr-ept-federated
    - Flux world maps for electrons (R.112)
    - High-latitude/polar electron flux survey (R.160)
    - High-latitude/polar proton flux survey (R.161)
    - Total ionizing dose estimation at LEO (R.167)
    - Total non-ionizing dose estimation at LEO (R.168)
- RB-IND Radiation belt activity indices for surface and internal charging (R.177): https://swe.ssa.esa.int/onera-rb-ind-federated
- SaRIF: https://swe.ssa.esa.int/sarif-federated
    - SaRIF GOES-16 Radiation Environment (R.145)

- SaRIF Slot Region Radiation Environment (R.154)
    - SaRIF GOES-16 Internal Charging Current (R.143)
    - SaRIF GIOVE-A Internal Charging Current (R.149)
    - SaRIF Slot Region Internal Charging Current (R.152)
    - MOSWOC high energy electron forecast for geostationary orbit (R.155)
- SWIFF Plasmasphere (SPM) electron density and temperature distribution model (R.136): https://swe.ssa.esa.int/bira-swiff-federated
- SREM: https://swe.ssa.esa.int/pb-srem-federated
    - Time series of PROBA-1/SREM radiation rates (R.118)
    - Time series of Integral/SREM radiation rates (R.119)

I-ESC:

- DLR/IMPC Near-real-time map of the Total Electron Content (TEC) for the European region (I.101b): https://swe.ssa.esa.int/impc-federated
- DLR/IMPC Maximum Usable Frequency for skip-distances of 750 km (MUF750) (I.139): https://swe.ssa.esa.int/impc-federated
- NMA: https://swe.ssa.esa.int/rtim-federated
    - ROTI@Ground maps (Fennoscandia) (I.109b)
    - VTEC maps (Northern Europe) (I.107)
    - σφ maps (Northern Europe) (I.110b)
- NOA EIS: https://swe.ssa.esa.int/dias-federated
    - Nowcast European maps of foF2 (based on the upgraded SIRMUP model) (I.115)
    - Alerts for ionospheric disturbances in the European sector (I.118)
- NOA TechTIDE: https://swe.ssa.esa.int/techtide-federated
    - GNSS TEC gradient (I.143)
    - LSTID detector maps (I.144)

G-ESC:

- FMI: https://swe.ssa.esa.int/fmi-federated, selected figures from:
    - Maps for power and pipeline operators (G.111)
    - products Pipe-to-soil voltage (PSV) (G.114)

- DTU's PCN index (G.144): https://swe.ssa.esa.int/dtu-pcn-federated
- DTU's Magnetogrammes from North(West) Europe and Greenland (G.101): https://swe.ssa.esa.int/nrt-mag-federated
- DTU's GIC indicator plots for Greenland and Northern Europe (G.159): https://swe.ssa.esa.int/dMAG_dt-federated
- DTU's K-index from magnetometer stations in north Europe (G.102): https://swe.ssa.esa.int/dtu-k-federated
- BGS: Peak Geomagnetically Induced Current (GIC) for Scotland, England, Wales and the UK (G.148): https://swe.ssa.esa.int/BGS-federated
- GFZ: Nowcast Hp30 index (G.154a) https://swe.ssa.esa.int/gfz-hpo-federated
- IRF: https://swe.ssa.esa.int/irf-federated
    - Forecast of Kp (G.134)
    - Forecast of Dst (G.135)
    - AE, AU and AL forecast (G.145)
    - Auroral data from Kiruna (G.146)